

Changing sources of magma generation beneath intra-oceanic island arcs: An insight from the juvenile Kohistan island arc, Pakistan Himalaya

Stella M. Bignold^{*}, Peter J. Treloar, Nick Petford

Centre for Earth and Environmental Science Research, School of Earth Sciences & Geography, Kingston University, Penrhyn Road, Kingston-upon-Thames, Surrey KT1 2EE, UK

Received 1 December 2004; received in revised form 13 January 2006; accepted 14 February 2006

Abstract

The Kohistan arc, situated in the Pakistan Himalaya, is a Cretaceous intraoceanic island arc which was initiated during the northward movement of the Indian Plate. The arc was sutured to Asia at ca. 100 Ma. It was subsequently tilted northward when underplated by Indian continental crust during the early stages of India–Asia collision. Deep erosion of this tilted section provides a spectacular section through the whole arc sequence and offers a profound insight into the mechanisms of early stages of arc formation. Geochemical analysis and rare earth element modelling of basaltic sequences which date from the intraoceanic stages of arc development allow identification of three main magma source types in the mantle beneath the juvenile arc. The ‘E-type’ Kamila Amphibolites, with a MORB-type chemistry, form the intraoceanic basement to the arc. The ‘D-type’ Kamila Amphibolites are the earliest of the arc volcanic rocks. These were extracted from a primitive spinel-bearing mantle source, above a north-dipping subduction zone. The stratigraphically younger basalts of the Jaglot Group and Ghizar Formation of the Chalt Volcanic Group were derived from partial melting of a garnet-bearing source at greater depth. The Hunza Formation of the Chalt Volcanic Group contains the youngest mafic volcanic rocks of the intraoceanic arc. Although coeval with the Ghizar Formation of the Chalt Volcanic Group, they were generated by melting of a depleted, spinel-bearing mantle source rock and were erupted into a spatially and temporally restricted back-arc basin developed behind the volcanic front. The Chalt Volcanic Group was therefore formed from two different, adjacent, mantle source regions active at the same time. Results of REE modelling are consistent with models for intraoceanic arc formation in which the earliest volcanic rocks are derived from shallow level spinel-bearing peridotite, and later ones from a deeper garnet-bearing source. This is consistent with the melt region becoming deeper with time as subduction continues. A two-stage model is proposed for the back-arc basalts of the Hunza Formation in which a mantle source, depleted from a previous melting event, is underplated beneath the arc and later remelted during decompression as a consequence of extension and rifting of the arc.

© 2006 Elsevier B.V. All rights reserved.

Keywords: Kohistan; Geochemistry; Rare earth element modelling; Stratigraphy; Subduction

^{*} Corresponding author. Fax: +44 20 8547 8850.

E-mail address: s.bignold@kingston.ac.uk (S.M. Bignold).

1. Introduction

The Kohistan arc, located in NW Pakistan, was initiated in the Neotethys Ocean during the Cretaceous as an intraoceanic island arc developed above a N-dipping subduction zone (Tahirkheli et al., 1979; Coward et al., 1987; Khan et al., 1993; Treloar et al., 1996; Burg et al., 1998; Bignold and Treloar, 2003). The arc was subsequently sutured to Asia between 104 Ma (Pettersson and Windley, 1985) and 85 Ma (Treloar et al., 1996), when it became an Andean-type volcanic margin. The arc was structurally telescoped along N-dipping thrusts during suturing and subsequent underthrusting by the leading edge of continental India. As a result, a full stratigraphic succession from the base of the arc to its stratigraphic top can now be traversed along accessible valleys. The opportunity therefore arises to trace temporal and spatial changes in volcanic style, chemistry and magma source regions through the complete life of the arc from its initiation as a juvenile intraoceanic island arc through its evolution and eventual suturing with Asia to become a continental margin arc.

Much geochemical data have been published from rock suites throughout the accessible regions of Kohistan (Jan and Howie, 1981; Pettersson and Windley, 1985; Jan, 1988; Khan et al., 1989; Treloar et al., 1989; Jan and Windley, 1990; Pettersson et al., 1990; Pettersson and Windley, 1991, 1992; Sullivan, 1992; George et al., 1993; Khan et al., 1993; Pettersson et al., 1993; Sullivan et al., 1993; Khan et al., 1996, 1997; Bignold and Treloar, 2003). This paper presents new stratigraphic and geochemical data for volcanic successions in both the eastern and western parts of the arc. The new geochemical data supplement previously published data and include complete rare earth element datasets.

Rare earth element modelling is used to identify potential magma sources and suggest the degree of partial melting in the mantle wedge beneath the arc, with the aim of determining changes in magma source regions as the juvenile arc evolved. The results of modelling each volcanic succession across the arc are combined with stratigraphic and geochemical analysis to formulate a model for magma generation beneath the arc from its initiation until suturing with Eurasia.

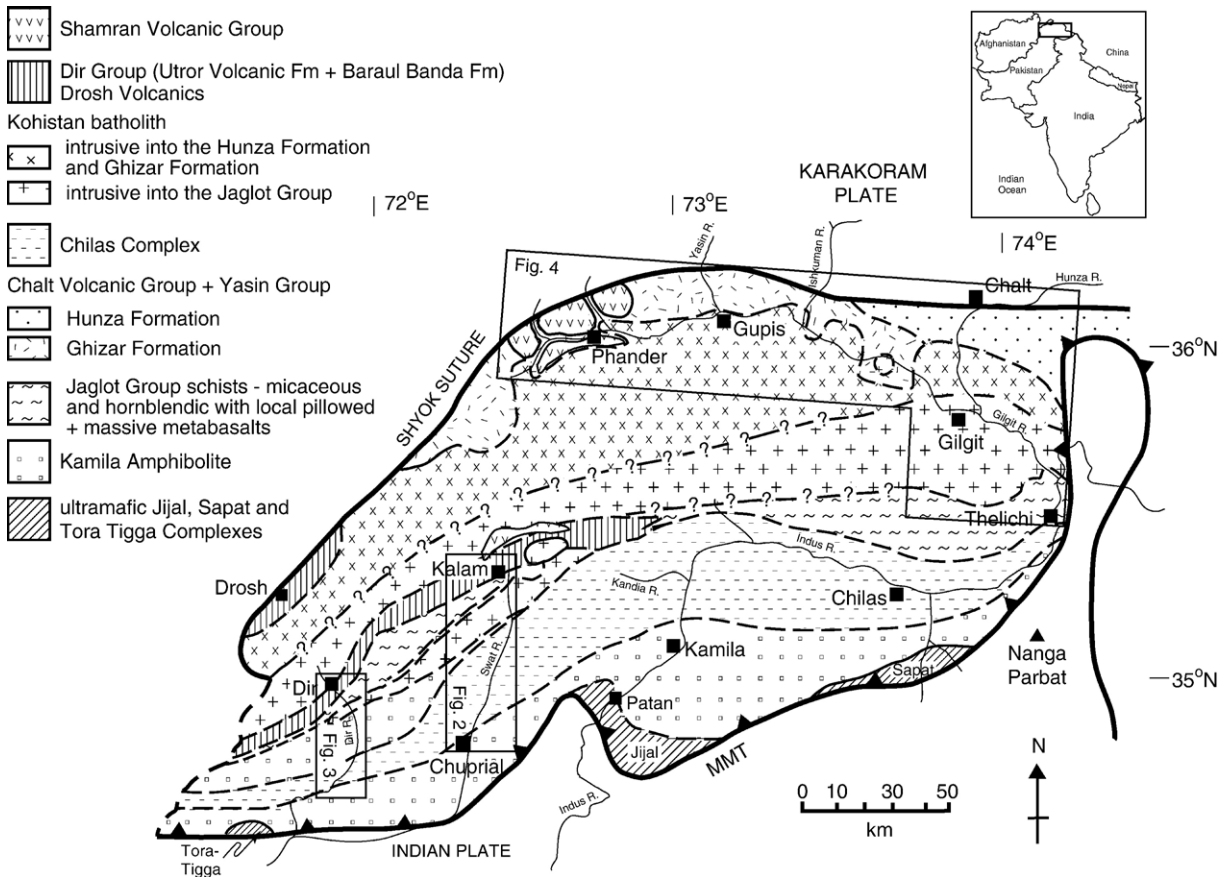


Fig. 1. Geological sketch map of Kohistan. Boxes denote sampling areas.

2. Outline geology of the Kohistan arc

The rocks of the Kohistan island arc trend generally east–west (Fig. 1), and dip northward. The arc is bounded to the north by the Shyok Suture, along which it is sutured

to Asia, and to the south by the Main Mantle Thrust (MMT), the western continuation of the Indus–Tzangpo Suture Zone along which it was thrust southward over continental India in the early Tertiary (Coward et al., 1982; Corfield et al., 2001.). It is bounded to the east by the

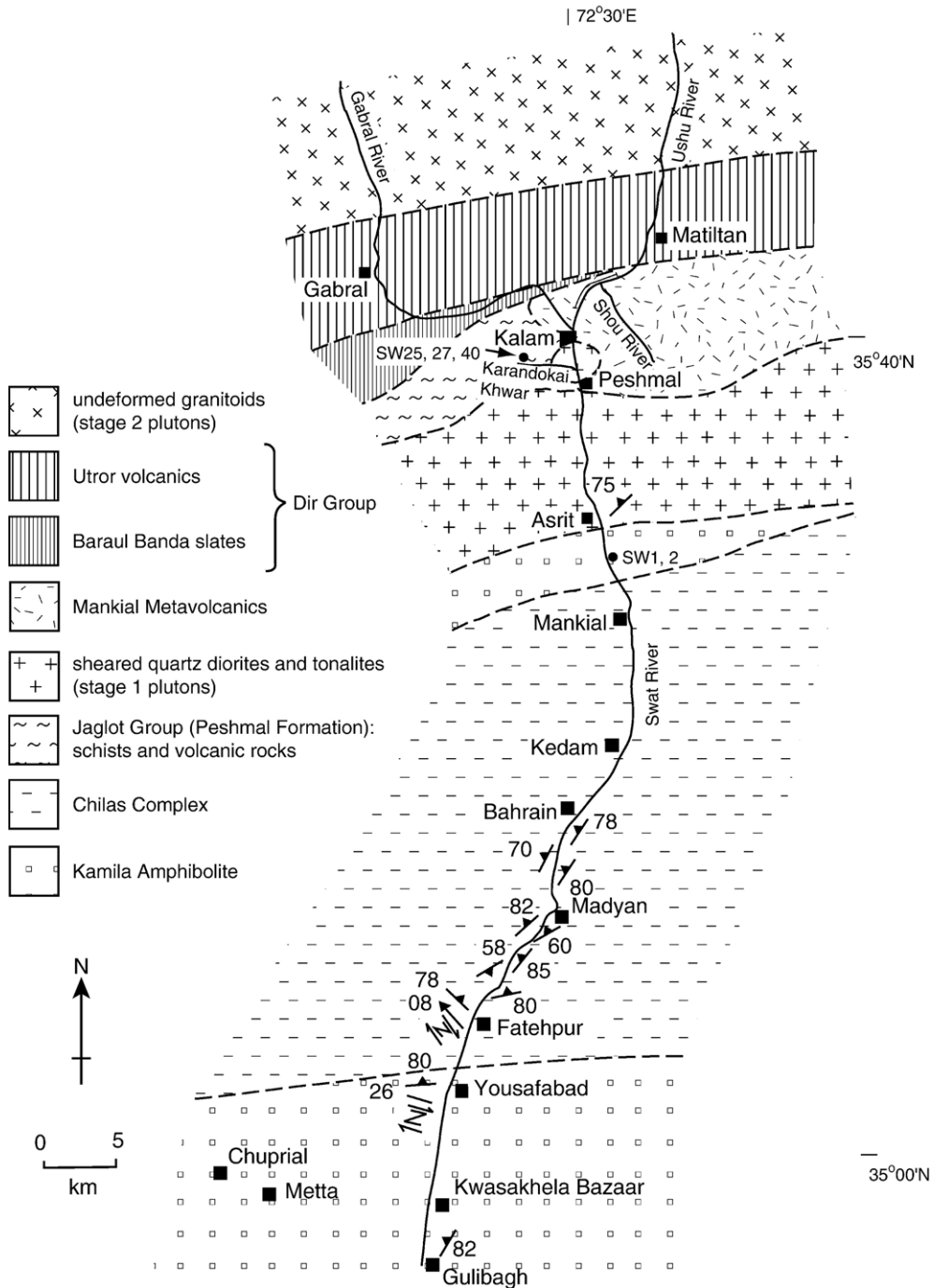


Fig. 2. Geological sketch map of the Swat valley, Kohistan, showing sample locations (modified from Treloar et al., 1996).

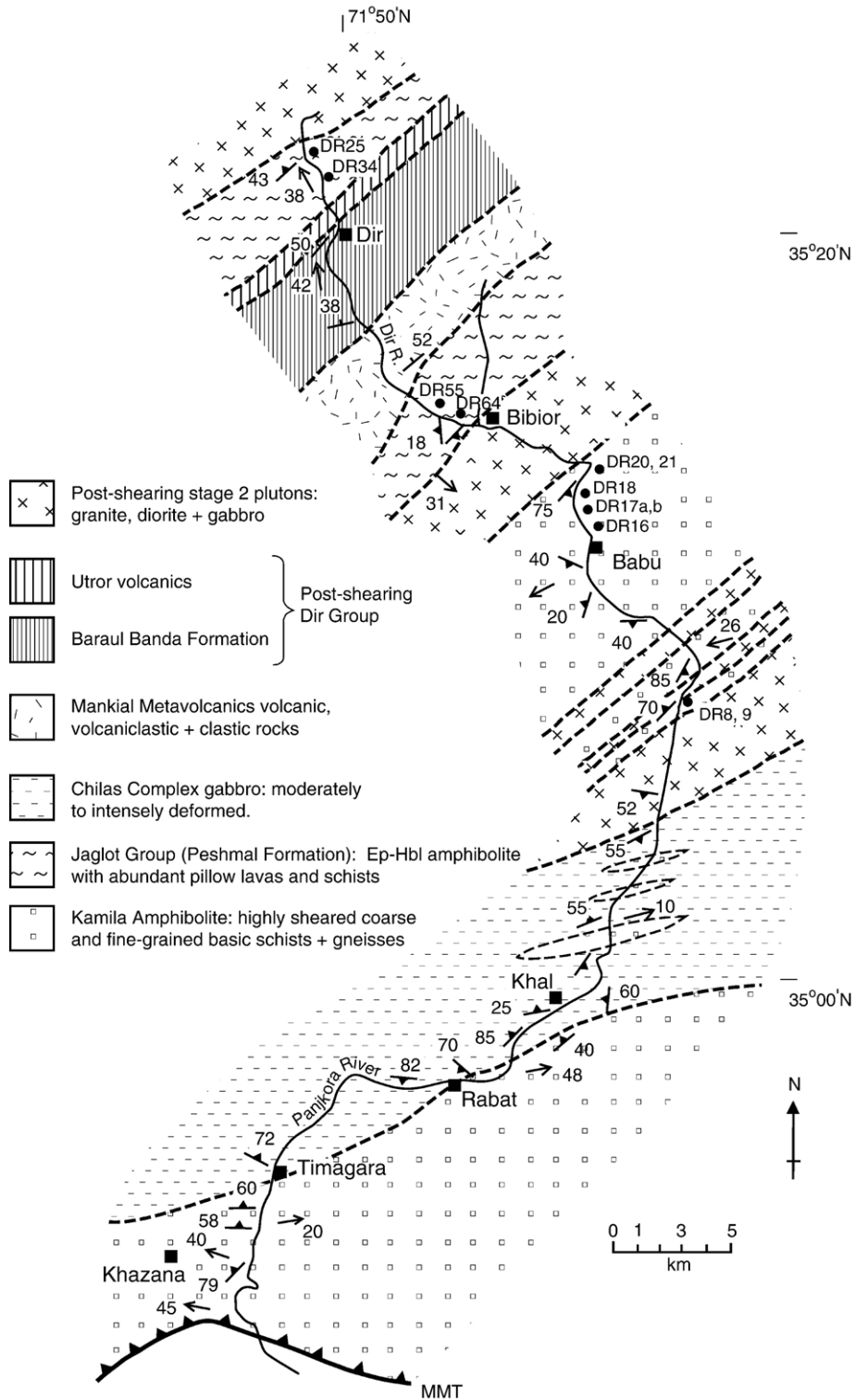


Fig. 3. Geological sketch map of the Panjkora and Dir valleys, Dir District, Kohistan, showing sample locations (modified from Treloar et al., 1996).

Raikot–Sassi fault zone (Coward et al., 1986), which separates the arc from the Indian Plate gneisses of Nanga Parbat, tectonically exhumed from beneath the arc rocks during the Pliocene.

Several distinct lithologies have been identified within the arc. A series of layered mafic and ultramafic intrusive cumulate bodies, the Jijal, Sapat and Torra Tigga complexes, occur along the southern margin of the arc, in the immediate hanging wall of the MMT (Ahmed and Chaudhry, 1976; Jan and Howie, 1981; Jan et al., 1983; Jan and Windley, 1990; Jan and Tahirkheli, 1990; Miller et al., 1991; Jan et al., 1992, 1993; Khan et al., 1998) (Fig. 1). Amongst these bodies, the Jijal Complex has a magmatic age of 118 ± 12 Ma with a subsequent granulite facies metamorphic overprint at about 100 Ma (Anczkiewicz and Vance, 2000; Yamamoto and Nakamura, 2000).

Three distinct volcano–sedimentary sequences are exposed within the arc. From south to north these are the Kamila Amphibolites, the Jaglot Group and the Chalt Volcanic Group. The Kamila Amphibolites (Fig. 1) extend E–W across the southern part of the arc, and have been studied in detail in the Indus and Swat valleys of central Kohistan (Jan, 1970, 1979, 1988; Treloar et al., 1990, 1996) and in south-east Kohistan in the Thak valley (Khan et al., 1998). They are dominantly composed of mafic rocks, both extrusive and intrusive, but with ultramafic, dioritic, tonalitic, granitic and trondhjemitic plutons, and rare sediments. The rocks have been metamorphosed to amphibolite facies, and, in

the Indus valley, are strongly sheared and deformed. The outcrop of the Kamila Amphibolite Belt widens westward so that in the Dir valley it has a cross-strike width of about 35 km (Figs. 1–3).

The Jaglot Group lies to the north of the Kamila Amphibolite Belt (Figs. 1–3) and was recognised as a major stratigraphic unit by Khan et al. (1994) and Treloar et al. (1996). It comprises a belt of volcanoclastic schists interbedded with metavolcanic rocks and extends E–W across the arc. It includes the Gilgit Formation, Gashu Confluence Volcanic Formation and Thelichi Volcanic Formation (Khan et al., 1994) which are exposed in the Indus valley to the southwest of Gilgit, the Majne Volcanic Formation to the S of Gilgit (Ahmed et al., 1977; Khan et al., 1994, 1996, 1997), and the Peshmal Schists (Jan, 1970; Jan and Mian, 1971; Khalil and Afridi, 1979; Sullivan, 1992) exposed in the Dir and Swat valleys in the west of the arc (Treloar et al., 1996). The northern margin of the Jaglot Group is intruded by the Kohistan Batholith across the length of the arc.

The Chalt Volcanic Group and the Yasin Group (Figs. 1, 4) crop out in an arcuate belt along the northern margin of the arc to the south of the Shyok Suture (Pettersen et al., 1990; Pettersen and Windley, 1991; Pettersen and Treloar, 2004). The Chalt Volcanic Group lies stratigraphically above the Jaglot Group, although both are intruded by granitoids of the Kohistan Batholith. The Chalt Volcanic Group has been divided into the Ghizar and Hunza Formations by Pettersen and Treloar (2004). The Hunza Formation has been

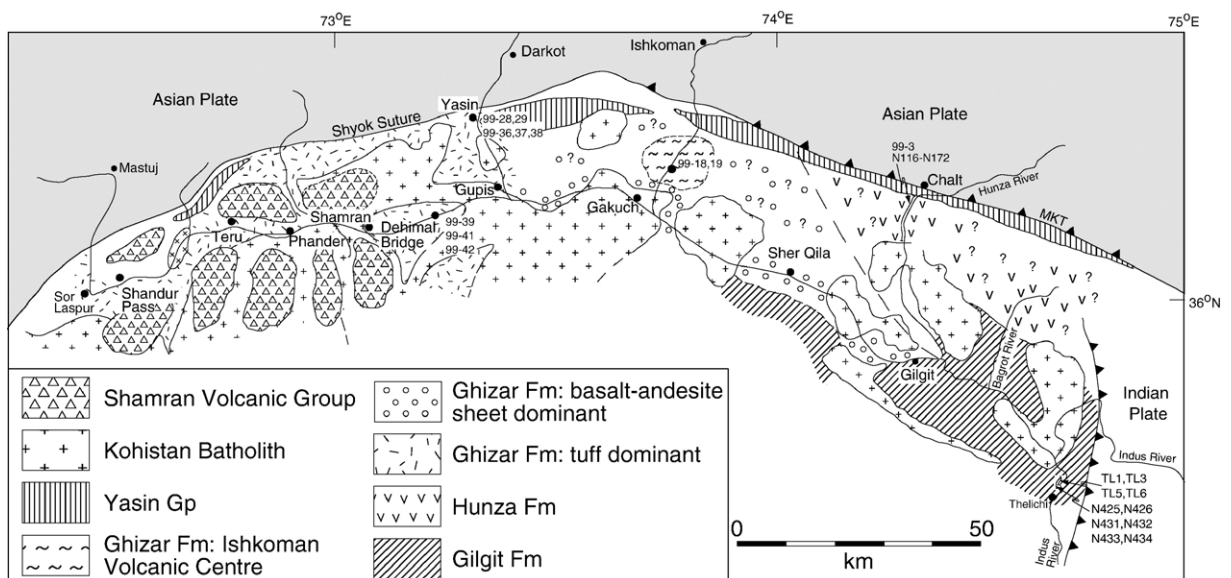


Fig. 4. Geological sketch map of northern Kohistan, showing sample locations (modified from Pettersen and Treloar 2004).

interpreted as a back-arc basin (Treloar et al., 1996; Rolland et al., 2000; Robertson and Collins, 2002; Bignold and Treloar, 2003). Rocks correlated with the Chalt Volcanic Group exposed to the east of the Nanga Parbat syntaxis carry a post-Valanginian fauna (Robertson and Collins, 2002).

The Chilas complex is a mafic to ultramafic, calc-alkaline intrusive body, which extends for 300 km E–W along the length of the arc, with a maximum width of 40 km (Khan et al., 1989) (Fig. 1). In the west of the arc, in the Dir valley, it is intrusive into the Kamila Amphibolites (Sullivan et al., 1993; Treloar et al., 1996). By contrast, in the east of the arc it is intrusive into the contact between the Jaglot Group to the north and the Kamila Amphibolites to the south (Fig. 1). It consists of massive gabbro-norites, with minor discordant dykes and intrusive bodies of a mixed dunite–peridotite–pyroxenite–anorthosite association (Jan, 1979; Jan and Howie, 1981). In the Indus Valley its northern margin contains abundant xenoliths of strongly deformed schists of the Jaglot Group (Treloar et al., 1996) which dates its emplacement as post-dating suturing of the arc to Asia. The southern margin, which lies on the hanging wall of the Kamila Shear Zone, is metamorphosed to amphibolite facies. The Chilas complex gabbro-norites in Upper Swat have a U–Pb zircon age of ~85 Ma (Zeitler et al., 1981; Zeilinger et al., 2001). A Sm–Nd age of 69.5 ± 9.3 Ma has been obtained from a “granulite facies” body of the Complex (Yamamoto and Nakamura, 1996).

The Kohistan Batholith (Fig. 1) forms part of the Trans-Himalaya Batholith and is intrusive into both the Chalt Volcanic Group and the Jaglot Group. On the basis of Rb–Sr whole-rock isochron ages, Petterson and Windley (1985, 1991) identified three distinct stages of emplacement of the Kohistan Batholith. Stage 1 plutons, which include the deformed Matum Das tonalite, were emplaced between 110 and 90 Ma, prior to suturing of the arc to Asia. Stage 2 plutons, with undeformed low-to-high-K calc-alkaline gabbros and diorites (with hornblende cumulates), and granodiorites were emplaced between 85 and 40 Ma. Stage 3 plutons were emplaced as granite sheets comprising biotite ± muscovite ± garnet leucogranites at about 30 Ma (George et al., 1993). Both Stages 2 and 3 were emplaced after suturing with Asia.

3. Field relations and geochemistry

In this study, samples of basaltic and andesitic volcanic rocks from all of the volcano–sedimentary groups have been analysed for major, trace and rare earth elements. Some samples from the Chalt Volcanic

Group, previously analysed by Petterson and Windley (1991) and from the Kamila Amphibolites previously analysed by Khan et al. (1997), were re-analysed in order to generate complete rare earth element datasets. Sample locations are plotted in Figs. 2–4.

Samples were ground to fine powder in an agate ball mill, taking care not to include any veined or weathered material, and all powders, including international reference standards, were oven-dried overnight at 105 °C. Lithium metaborate (LiBO_2) fusions were prepared, including blanks. Powders were weighed and thoroughly mixed with LiBO_2 , which had low La contamination. Each mixture was transferred to a carbon crucible and fused in a muffle furnace at 1050 °C. The melts were poured into polythene screw-top bottles containing 0.8 M HNO_3 , and the solutions were stirred until dissolved. The solutions were filtered into volumetric flasks and made up to an 0.5 M HNO_3 solution with deionised water. They were immediately transferred to new polypropylene bottles for storage. Analysis took place within 1 week of preparation to avoid hydrolysis and possible precipitation during storage. Major elements were analysed using the Horiba Jobin Yvon Ultima 2C ICP-AES, and trace and rare earth elements at the NERC ICP-MS Facility at Kingston University using the VG Elemental Plasma-Quad 2+ STE. Analytical precision and accuracy during analysis by ICP-AES were monitored using an international reference standard after every five samples. Analysis by ICP-MS requires that the solutions are diluted a further 25-fold prior to analysis. The instrument was calibrated using synthetic mixed-element standard solutions. Analytical precision and accuracy during ICP-MS analysis were monitored using international standard reference materials run at the same time as the samples. An internal standard solution was analysed after every five samples to monitor any drift, and all analyses were corrected for drift. The lower limits of detection (Table 1) were calculated to a 95% confidence level of 3 standard deviations (3σ) of the data. Data below this level were discarded.

Radiogenic isotope data for Sr, Nd and Pb were obtained at NIGL, Keyworth (Bignold and Treloar, 2003). Samples were carefully selected on two criteria. Thin section analysis enabled us to exclude any samples showing significant degrees of post-metamorphic hydration. Secondly, geochemical analytical data were used to ensure that adequate levels of Sr, Nd and Pb were present for isotopic analysis. Analytical procedures followed were those published for Sr and Nd by Royse et al. (1998) and for Pb by Kempton (1995). Sr and Pb were run as the metal species on single Ta and single Re

Table 1
Table of geochemical analyses for the Kamila Amphibolites

	D-type ^e												E-type ^e					LLD	
	SW3	SW2	DR16	DR21	DR8	DR17b	DR20	DR17a	DR9	DR18	A125 ^a	A119 ^a	A121 ^a	A086 ^a	A093 ^a	A083 ^a	002–		001–
SiO ₂	48.14	51.26	47.05	49.12	50.41	50.76	51.23	51.24	51.65	51.72	48.72	49.54	50.26	47.98	48.76	51.19	51.45	52.61	
TiO ₂	1.36	0.85	0.69	1.11	0.89	0.96	0.72	0.91	0.57	0.93	0.75	0.69	0.47	2.13	1.86	2.24	2.20	2.19	
Al ₂ O ₃	16.09	12.12	13.30	18.88	15.97	19.23	16.59	14.57	16.38	18.11	19.11	15.90	16.36	14.44	14.71	14.31	14.36	13.94	
FeOt	11.26	8.27	8.14	11.47	8.40	7.64	7.55	8.88	7.07	8.23	8.23	8.17	8.04	12.67	11.75	13.20	13.21	12.21	
MnO	0.22	0.14	0.13	0.14	0.16	0.15	0.14	0.14	0.15	0.12	n/d	n/d	n/d	n/d	n/d	n/d	0.14	0.22	
MgO	7.43	13.07	12.48	5.58	8.12	5.46	8.63	8.85	7.72	5.78	6.50	11.17	8.18	6.11	6.90	5.11	3.30	3.24	
CaO	9.71	11.11	12.13	9.41	10.36	9.63	9.74	11.32	9.83	9.19	12.01	9.83	12.28	11.64	11.82	9.63	10.68	10.29	
Na ₂ O	2.58	1.18	1.30	3.16	3.09	3.47	2.40	3.10	3.16	3.87	2.52	3.22	2.81	3.09	2.66	2.40	2.49	2.37	
K ₂ O	0.09	0.55	0.83	0.88	0.95	1.25	0.17	0.49	1.02	0.99	1.06	0.38	0.57	0.32	0.08	0.26	0.23	0.29	
P ₂ O ₅	0.13	0.20	0.16	0.04	0.16	0.17	0.12	0.10	0.08	0.19	0.17	0.19	0.12	0.21	0.17	0.19	0.29	0.28	
V	287	236	145	259	164	188	178	201	138	195	169	149	147	287	214	298	n/d	n/d	0.7
Cr	81.3	1002	841	7.62	225	179	313	399	315	277	173	46.8	153	186	174	25.9	13.7	24.3	2.2
Ni	40.9	315.7	194	17.4	118	57.9	156	145	102	76.7	74.5	178.3	59.7	82.2	70	35.1	5.7	5	2.7
Cu	9.5	59.8	59	69.8	33	90.3	19.9	59.9	60.3	28	bdl	bdl	6.1	bdl	bdl	9.1	22.4	52.3	2
Zn	122	69.7	47.1	91.6	58.9	48.9	61.4	53.6	70.7	64.2	53.2	40.7	39.8	99.3	65.3	71.6	42.1	57.4	3.4
Rb	6.1	11.8	13.2	20.4	10.8	29.5	3.7	5.1	16.5	15.6	21.1	7.8	7.1	2	1	2.4	0.6	1.8	0.6
Sr	367	162	93	304	125	218	152	132	174	156	227	206	229	110	136	134	334	226	0.3
Y	25.9	14.1	13.7	24.3	15.8	20.5	15.7	18.2	12.4	21.5	3.8	2.3	bdl	28.1	19.6	31.3	59.3	66.3	0.2
Zr	45.1	33.8	26	30.7	37.8	51.3	38.2	45.2	32.8	56.7	37.3	30.8	17.1	105.3	84	109.7	185.3	235	0.4
Nb	2.68	1.49	0.35	1.31	1.95	4.31	0.97	3.2	1.76	1.47	4.73	3.54	1.53	5.35	4.07	4.8	8.08	8.78	0.21
Ba	49	104	52	65.6	98.4	163	17.2	46.1	108	48.2	163	38.7	50.4	35.7	15.5	41.1	0.8	5.6	1.2
Hf	1.87	1.23	0.98	1.28	1.45	1.78	1.22	1.59	1.21	1.54	1.73	1.19	0.76	4.12	2.90	3.40	5.04	6.47	0.07
Ta	0.13	0.18	0.26	0.11	0.22	0.19	0.14	0.31	0.15	0.14	1.23	1.54	1.47	0.68	0.56	0.53	1.93	3.15	0.05
Pb	1.21	0.58	bdl	0.79	bdl	bdl	bdl	bdl	bdl	bdl	2 ^a	2 ^a	2 ^a	2 ^a	2 ^a	2 ^a	n/d	n/d	0.27
Th	bdl	1.00	0.45	bdl	1.03	0.34	0.69	0.45	0.96	0.28	2.25	0.77	0.59	0.82	0.41	0.87	0.76	0.98	0.04

U	bdl	0.38	0.33	bdl	bdl	bdl	0.21	bdl	bdl	bdl	0.46	0.1	0.1	0.21	bdl	0.45	0.33	0.47	0.07
La	4.14	3.98	2.87	3.11	6.02	4.29	3.86	3.32	4.33	3.64	10.00	25.70	2.98	7.30	4.86	5.28	5.04	6.74	0.09
Ce	14.20	11.70	6.19	9.08	12.97	9.68	9.56	7.90	10.17	10.14	21.33	12.17	6.97	19.43	14.33	15.67	27.83	30.30	0.12
Pr	2.65	1.75	1.16	1.47	1.67	1.57	1.27	1.18	1.33	1.40	2.47	1.74	0.98	3.12	2.07	2.26	4.38	4.59	0.05
Nd	13.13	8.19	5.35	8.06	7.85	7.52	6.47	6.52	7.60	8.72	10.13	8.78	4.65	16.23	11.83	15.17	22.67	25.27	0.04
Sm	4.04	2.38	1.73	3.15	2.36	1.63	2.06	1.62	2.11	2.60	2.87	2.50	1.56	5.18	3.78	4.84	6.48	7.73	0.03
Eu	1.29	0.80	0.84	0.91	0.73	1.07	0.72	0.76	0.72	0.91	0.84	0.87	0.56	1.73	1.50	1.60	2.47	2.74	0.01
Gd	4.62	2.49	1.77	4.23	3.04	2.72	2.78	1.27	2.11	3.28	1.74	1.61	0.82	4.94	4.50	5.80	9.14	10.80	0.13
Tb	0.82	0.35	0.52	0.62	0.46	0.63	0.42	0.55	0.33	0.55	0.09	bdl	bdl	0.79	0.65	1.59	1.55	2.03	0.02
Dy	5.49	3.08	2.76	4.93	3.49	3.97	2.94	2.70	1.96	3.89	2.92	2.45	2.00	7.16	6.19	7.53	10.77	11.27	0.08
Ho	1.04	0.54	0.85	0.98	0.73	0.61	0.65	0.73	0.48	0.85	0.64	bdl	0.42	1.65	1.41	1.58	2.26	2.31	0.04
Er	3.01	1.83	1.94	2.63	1.88	2.60	1.66	1.81	1.44	2.30	1.68	1.62	1.37	4.60	4.30	4.58	6.23	7.17	0.09
Tm	0.36	0.21	0.38	0.43	0.28	0.22	0.27	0.35	0.22	0.39	0.23	0.17	0.17	0.72	0.55	0.74	1.08	1.11	0.01
Yb	2.79	1.43	1.71	2.42	1.99	1.86	1.48	2.44	1.34	2.58	1.94	1.74	1.25	4.52	3.57	5.19	5.71	7.04	0.08
Lu	0.41	0.35	0.37	0.40	0.29	0.31	0.29	0.31	0.23	0.51	0.28	0.25	0.15	0.63	0.44	0.59	0.94	1.07	0.01
⁸⁷ Sr/ ⁸⁶ Sr	0.70446										0.70467	0.70417	0.70467	0.70384	0.70366	0.70388			
¹⁴³ Nd/ ¹⁴⁴ Nd	0.51274										0.51274	0.51284	0.51283	0.51299	0.51301	0.51302			
εNd ₁₂₀	2.19										2.90	4.70	4.20	7.00	7.40	7.40			
²⁰⁶ Pb/ ²⁰⁴ Pb	18.469										18.462	18.073	18.033	18.128	18.087	17.973			
²⁰⁷ Pb/ ²⁰⁴ Pb	15.611										15.586	15.527	15.535	15.497	15.456	15.561			
²⁰⁸ Pb/ ²⁰⁴ Pb	38.628										38.644	38.170	38.039	38.080	37.979	37.951			
Mg#	0.54	0.74	0.73	0.46	0.63	0.56	0.67	0.64	0.66	0.56	0.58	0.71	0.64	0.46	0.51	0.41	0.50	0.51	
(Ce/Yb) _N	1.32	2.12	0.94	0.97	1.68	1.35	1.67	0.84	1.96	1.02	2.84	1.81	1.44	1.11	1.04	0.78	1.26	1.11	
Eu/Eu*	0.91	1.00	1.47	0.76	0.84	1.55	0.91	1.62	1.04	0.96	1.15	1.33	1.51	1.05	1.11	0.92	0.98	0.92	

Samples prefixed with 'A' are from Khan et al. (1997) 74°00'N, 35°20.4'E. Sample locations are shown in Figs. 2 and 3. LLD=lower limits of detection; Eu/Eu*=Eu_N/√[(Sm)_N·(Gd)_N]; Mg#=100 [Mg²⁺/(Mg²⁺+Fe²⁺)].

^a Analyses from Khan et al. (1997).

Table 2
Table of geochemical analyses for the Jaglot Group

	Gashu Confluence Volcanic Formation										Peshmal Formation						
	N433	TL5	N426	N432	N431	N434	N425	TL3	TL1	TL6	DR64	DR34	SW27	SW25	SW40	DR55	DR25
SiO ₂	48.32	51.16	55.46	56.66	56.9	57.46	60.21	60.51	61.05	61.57	45.71	47.40	47.41	48.06	48.34	51.64	51.86
TiO ₂	1.51	1.07	1.21	0.75	0.7	0.75	0.18	0.56	0.18	0.14	0.67	0.90	0.82	0.74	0.91	0.70	0.83
Al ₂ O ₃	17.09	16.33	14.37	15.9	16.29	13.79	13.36	18.14	13.19	16.52	15.10	16.92	13.07	13.30	13.25	16.19	17.50
FeO _t	9.71	9.77	2.53	1.93	1.95	1.86	1.49	1.48	1.46	1.05	41.82	11.39	9.63	9.53	10.13	10.29	9.34
MnO	0.17	0.19	0.23	0.14	0.17	0.18	0.09	0.19	0.08	0.09	0.25	0.33	0.19	0.22	0.20	0.24	0.38
MgO	7.71	7.36	4.59	5.66	6.17	7.01	5.91	2.38	5.05	4.75	11.77	1.83	13.43	12.92	12.90	6.77	5.79
CaO	9.85	9.39	6.87	9.84	6.35	6.92	7.94	6.86	11.12	10.51	10.83	12.54	11.66	12.17	11.49	12.19	9.86
Na ₂ O	3.38	2.79	3.29	3.32	6.2	4.31	1.41	3.43	0.55	0.86	1.29	1.99	0.99	0.67	0.69	0.71	3.81
K ₂ O	0.41	0.44	0.86	0.34	0.26	1.34	0.9	0.64	0.03	bdl	1.07	3.52	1.16	1.10	0.93	1.55	1.21
P ₂ O ₅	0.24	0.28	0.15	0.14	0.12	0.13	0.08	0.18	0.06	0.02	0.22	0.10	0.17	0.13	0.13	0.30	0.11
V	151	168	359	208	262	218	195	58.6	158	137	237	221	174	146	193	231	170
Cr	85.3	280	57.2	80.9	66	107	132	bdl	126	172	615	74.5	703	701	622	150	70.8
Ni	78.4	83	37.1	42.9	61.1	56.3	56.5	bdl	65.4	50.8	168	36.8	188	196	181	47.5	20.2
Cu	25.9	111	28.4	50.7	48.1	82.1	80.6	9.1	24.9	65.2	61.6	20.2	bdl	bdl	2.1	5.3	7.6
Zn	48.5	70.7	89	50.1	60.1	72.1	40.2	74.4	50.5	42.3	103.6	77.9	52.6	62.3	74	140.7	90.4
Rb	6.11	6.27	25.7	3.87	0.49	30.8	2.42	21.8	3.03	bdl	29.9	112.3	33.1	39.1	32.67	71.53	28
Sr	321	311	202	162	31.8	86.7	58.2	393	41	66.4	142	140	60	69.9	105.7	343	276.7
Y	23.7	20	28.8	17.3	16.8	18.6	3.1	19.2	3.6	6.0	14.8	14.1	11.8	9.0	12.3	19.4	10.2
Zr	118	48	68.4	41.1	39.3	41.1	27.1	64.4	25.7	30.6	41.9	43.2	35.3	28	32.2	42	24.3
Nb	3.61	1.84	1.53	0.94	0.92	1.29	1.21	2.56	1.36	0.93	2.09	1.76	1.68	1.63	1.93	1.78	0.78
Ba	39.7	106	72.4	44.8	10.9	291	28.9	314	25.4	21.5	85.4	390	28.1	93.1	36.5	108.3	44.3
Hf	2.58	1.62	1.95	1.40	1.21	1.51	0.71	1.84	0.71	1.11	1.29	1.29	1.39	1.18	0.88	1.49	1.10
Ta	0.28	0.18	0.13	0.06	0.06	0.11	0.19	0.09	0.15	0.16	0.13	0.06	0.13	0.07	0.13	0.14	0.12
Pb	1.33	1.15	bdl	bdl	bdl	0.69	bdl	0.86	1.57	1.63	0.76	1.39	1.03	1.56	0.90	2.54	1.20
Th	0.41	0.95	0.54	0.37	0.67	0.38	1.71	1.59	1.42	2.19	1.81	0.64	1.68	1.11	1.01	1.63	0.35
U	bdl	0.39	bdl	bdl	bdl	bdl	bdl	0.66	0.53	0.81	0.46	0.26	0.44	0.27	0.36	0.53	0.21
La	6.70	7.01	3.49	2.31	3.18	1.67	2.40	8.25	3.26	5.10	9.61	4.38	6.73	4.61	5.01	9.48	2.58
Ce	18.30	17.10	9.93	6.62	6.74	6.25	5.95	19.40	7.20	10.30	20.03	8.91	14.73	10.16	10.80	19.33	6.61
Pr	2.79	2.49	1.73	1.14	1.02	1.15	0.68	2.64	0.75	1.11	3.06	1.31	1.97	1.34	1.38	2.68	0.99
Nd	14.20	10.60	9.22	6.41	5.70	6.82	2.76	12.30	2.50	3.98	13.07	5.58	9.15	5.34	7.12	12.00	4.96
Sm	3.69	3.64	2.86	2.41	1.96	2.36	bdl	3.07	0.91	1.38	2.48	1.72	2.68	1.84	2.75	4.14	1.64
Eu	1.47	1.22	1.02	0.74	0.73	0.84	0.22	1.14	0.36	0.12	1.07	0.58	0.48	0.41	0.60	0.70	0.79
Gd	4.37	2.85	3.91	2.68	2.71	3.12	0.61	3.35	0.97	1.28	2.94	2.58	2.51	2.09	2.68	3.33	1.96
Tb	0.73	0.61	0.72	0.48	0.50	0.54	0.09	0.47	0.12	0.20	0.51	0.40	0.39	0.32	0.44	0.48	0.40
Dy	4.93	3.85	5.15	3.52	2.45	4.01	0.66	3.79	0.91	1.09	2.60	2.74	2.99	2.02	2.29	3.77	1.91
Ho	0.92	0.82	1.09	0.73	0.72	0.84	0.13	0.67	0.11	0.18	0.62	0.52	0.47	0.48	0.56	0.64	0.56
Er	2.90	2.15	3.31	2.19	2.09	2.42	0.49	2.30	0.55	0.81	1.65	1.60	1.36	1.01	1.43	2.69	1.24
Tm	0.44	0.33	0.49	0.31	0.32	0.36	bdl	0.38	0.06	0.12	0.19	0.27	0.23	0.21	0.22	0.36	0.28
Yb	2.76	2.05	3.05	1.99	2.10	2.32	0.63	2.16	0.67	1.16	1.85	2.04	1.41	0.99	1.51	2.61	1.30
Lu	0.37	0.24	0.41	0.37	0.33	0.37	bdl	0.39	0.08	0.13	0.30	0.25	0.30	0.21	0.19	0.31	0.23
⁸⁷ Sr/ ⁸⁶ Sr	0.7	0.7				0.71				0.71							
¹⁴³ Nd/ ¹⁴⁴ Nd	0.51	0.51				0.51				0.51							
εNd ₁₂₀	6.44	4.17				6.17				-6.93							
²⁰⁶ Pb/ ²⁰⁴ Pb	18.19	18.45				18.33				18.5							
²⁰⁷ Pb/ ²⁰⁴ Pb	15.53	15.62				15.58				15.64							
²⁰⁸ Pb/ ²⁰⁴ Pb	38.18	38.63				38.4				38.65							
Mg#	0.59	0.57	0.42	0.54	0.56	0.60	0.61	0.39	0.58	0.64	0.66	0.22	0.72	0.71	0.69	0.54	0.52
(Ce/ Yb) _N	1.72	2.16	0.84	0.86	0.83	0.70	2.44	2.32	2.78	2.30	2.80	1.13	2.70	2.66	1.85	1.92	1.31
Eu/Eu*	1.12	1.16	0.93	0.89	0.97	0.95		1.09	1.17	0.28	1.21	0.84	0.57	0.64	0.68	0.58	1.35

bdl=below detection limits. Sample locations are shown in Figs. 2 and 3. Eu/Eu* = Eu_N/√[(Sm)_N·(Gd)_N]; Mg# = 100[Mg²⁺/(Mg²⁺ + Fe²⁺)].

Table 3
Table of geochemical analyses for the Hunza Formation of the Chalt Volcanic Group

	N116 low- Mg	N146 ^a high-Mg	N157 high-Mg	N133 low-Mg	N153 high-Mg	N156 high-Mg	N134 low-Mg	99-3 low- Mg	N161 high-Mg	N158 ^a high-Mg boninite	N172	N163	N169	N138 ^a high-Mg boninite	N121
SiO ₂	46.49	48.7	48.99	49.07	49.62	50.23	50.74	50.84	51.98	53.00	55.39	53.2	59.14	59.8	61.13
TiO ₂	0.56	0.42	0.23	0.28	0.32	0.23	0.33	0.31	0.21	0.21	0.37	0.26	0.36	0.23	0.56
Al ₂ O ₃	19.38	11.6	10.89	14.84	14.13	10.14	17.04	14.94	9.42	9.40	15.84	12.00	14.26	11.80	13.17
FeO _t	12.31	10.80	9.13	8.69	9.07	8.98	9.35	8.19	8.85	8.28	9.12	6.39	6.98	7.11	9.34
MnO	0.21	0.19	0.17	0.21	0.12	0.17	0.17	0.15	0.18	0.16	0.15	0.12	0.13	0.18	0.18
MgO	7.98	13.40	14.92	6.47	12.06	15.90	8.40	7.97	15.02	14.40	7.17	6.90	7.63	8.70	4.44
CaO	9.18	11.80	12.25	18.28	9.44	10.83	10.10	11.13	12.51	10.90	10.26	8.20	6.74	10.10	8.43
Na ₂ O	2.46	1.60	1.37	0.24	2.37	0.96	2.80	2.53	1.29	1.90	2.38	1.30	4.72	0.70	2.11
K ₂ O	0.67	0.25	0.20	0.04	1.09	1.17	1.15	1.19	0.29	0.11	0.05	1.16	0.42	0.20	0.20
P ₂ O ₅	0.06	0.03	0.04	0.09	0.06	0.03	0.02	0.03	0.04	0.03	0.08	0.03	0.05	0.04	0.09
V	288	182	191	343	186	151	226	n/d	138	135	181	136	159	164	358
Cr	89	1176	1340	422	633	1144	126	407	1495	1148	193	418	375	72	18
Ni	35	290	283	86.2	121	254	70.5	85.2	448	64.7	41.5	105	92	114.3	28
Cu	50.2	182	16.5	12.1	3.5	29.5	481	30.7	bdl	52.6	58.1	30.5	38.6	11.9	180
Zn	77.1	105.8	61.4	45.7	80.3	52.1	56.5	41.4	40.6	38.7	33.7	25.6	30.5	58.2	87.2
Rb	17.30	3.18	2.00	2.77	27.10	26.53	4.13	2.19	2.35	0.60	0.70	13.20	3.80	2.48	2.37
Sr	111	18.1	116.6	103	71.7	51.3	97.1	71.9	54.8	50.5	149	203	453	52.2	50.9
Y	16.1	6.7	10.9	8.2	7.0	5.4	5.7	6.7	5.5	4.8	8.0	7.5	8.4	6.2	10.4
Zr	14.8	33.7	12.4	12.8	18.9	12	15.1	17.3	13.3	13.3	27.8	14.6	24.1	19.1	22
Nb	0.46	1.05	0.46	0.66	0.36	1.00	1.04	0.65	bdl	0.30	0.59	0.33	0.55	0.74	0.95
Ba	35.2	4.65	7.91	1.68	49.1	89.8	14.9	17.7	8.68	10.9	10.6	46.1	32.6	10.4	6.5
Hf	0.51	0.95	0.35	0.31	0.45	0.45	0.46	0.45	0.56	0.51	0.76	0.52	0.81	0.63	0.55
Ta	0.09	0.13	0.11	0.13	0.12	0.23	0.12	1.29	0.09	0.05	bdl	bdl	bdl	0.14	0.22
Pb	5.00 ^a	4.00 ^a	4.00 ^a	0.32	bdl	4.00 ^a	6 ^a	n/d	6.00 ^a	5.00 ^a	bdl	2.00 ^a	7.00 ^a	5.00 ^a	8.00 ^a
Th	0.20	bdl	bdl	bdl	bdl	0.23	bdl	0.12	0.16	0.3	0.28	0.13	0.2	bdl	0.22
U	bdl	0.16	0.08	0.17	0.07	0.1	0.25	0.15	bdl	0.77	bdl	bdl	bdl	bdl	0.08

(continued on next page)

Table 3 (continued)

	N116 low- Mg	N146 ^a high-Mg	N157 high-Mg	N133 low-Mg	N153 high-Mg	N156 high-Mg	N134 low-Mg	99-3 low- Mg	N161 high-Mg	N158 ^a high-Mg boninite	N172	N163	N169	N138 ^a high-Mg boninite	N121
La	2.45	1.03	0.76	1.20	0.47	0.37	0.28	bdl	0.49	0.57	1.16	0.70	0.93	0.62	1.06
Ce	3.53	1.57	1.11	0.99	1.06	0.77	1.00	2.24	0.79	1.00	2.38	0.52	1.89	1.67	1.67
Pr	0.94	0.27	0.23	0.19	0.17	0.17	0.17	0.20	0.27	0.22	0.45	0.23	0.45	0.23	0.45
Nd	4.52	1.72	1.49	1.23	1.76	1.27	1.12	1.84	0.93	1.38	2.60	1.71	2.49	1.63	1.63
Sm	1.48	0.36	0.37	0.42	0.20	0.14	0.13	0.97	0.71	1.13	0.89	0.73	0.92	0.46	0.47
Eu	0.54	0.20	0.26	0.23	0.21	0.14	0.25	0.25	0.25	0.27	0.43	0.29	0.40	0.17	0.35
Gd	2.08	0.68	0.65	0.80	0.91	0.63	0.48	0.74	0.80	0.61	1.28	1.03	1.20	0.74	0.98
Tb	0.47	0.19	0.23	0.17	0.16	0.19	0.13	0.14	0.21	0.19	0.22	0.21	0.24	0.14	0.31
Dy	3.12	1.32	1.67	1.04	1.03	1.01	1.14	1.24	1.20	0.93	1.61	1.42	1.64	0.95	1.91
Ho	0.64	0.36	0.32	0.29	0.24	0.24	0.25	0.33	0.30	0.22	0.34	0.32	0.37	0.19	0.37
Er	2.05	0.97	1.06	0.80	0.78	0.66	0.70	1.02	0.75	0.66	1.08	1.07	1.07	0.70	1.10
Tm	0.25	0.20	0.17	0.13	0.12	0.14	0.10	0.18	0.17	0.15	0.16	0.18	0.16	0.10	0.17
Yb	1.96	1.49	1.09	0.93	0.96	0.85	0.60	0.61	0.81	0.76	1.15	1.28	1.44	0.79	1.18
Lu	0.25	0.22	0.17	0.15	0.11	0.15	0.12	0.13	0.20	0.16	0.23	0.21	0.21	0.12	0.19
⁸⁷ Sr/ ⁸⁶ Sr	0.705200	0.705251	0.705135						0.705715	0.705544		0.705593		0.705525	
¹⁴³ Nd/ ¹⁴⁴ Nd	0.512950	0.512960	0.513014						0.513035	0.513029		0.513026		0.512970	
εNd ₁₂₀	6.30	7.32	8.01						6.44	6.51		6.59		6.30	
²⁰⁶ Pb/ ²⁰⁴ Pb	18.243	18.277	18.318						18.207	18.147		18.091		18.283	
²⁰⁷ Pb/ ²⁰⁴ Pb	15.540	15.549	15.565						15.533	15.532		15.521		15.569	
²⁰⁸ Pb/ ²⁰⁴ Pb	38.224	38.236	38.169						38.135	38.108		38.048		38.315	
Mg#	0.51	0.64	0.72	0.54	0.66	0.74	0.59	0.63	0.75	0.76	0.59	0.66	0.64	0.69	0.43
(Ce/ Yb) _N	0.47	0.27	0.26	0.28	0.29	0.23	0.43	0.95		0.34	0.54	0.11	0.34	0.55	0.37
Eu/Eu*	0.94	1.24	1.62	1.21	1.51			0.91	1.01		1.23	1.02	1.16	0.89	1.58

Major element analyses for those marked with * are from Petterson and Windley (1991). n/d=not determined; bdl=below detection limits. Sample locations are shown in Fig. 4. $Eu/Eu^* = Eu_N / \sqrt{[(Sm)_N \cdot (Gd)_N]}$; $Mg\# = 100[Mg^{2+} / (Mg^{2+} + Fe^{2+})]$.

^a Major element analyses from Petterson and Windley (1991).

Table 4
Table of geochemical analyses for the Ghizar Formation of the Chalt Volcanic Group

	99-19	99-18	99-37	99-38	99-36	99-29	99-28	99-39	99-42	99-41	BHVO-1	AGV-1
	Ishkoman	Ishkoman	Yasin	Yasin	Yasin	Yasin	Yasin	Dehimal	Dehimal	Dehimal		
SiO ₂	48.64	49.52	50.52	54.99	54.52	56.12	59.52	59.66	60.70	61.46	50.85	58.35
TiO ₂	0.58	0.52	0.48	0.51	0.56	0.59	0.58	0.70	0.68	0.70	2.80	1.02
Al ₂ O ₃	13.57	14.30	14.67	14.91	14.26	17.65	17.38	15.95	16.35	16.46	13.61	16.86
FeO _t	9.53	8.87	8.48	8.17	9.14	8.35	7.32	6.09	4.81	4.74	12.12	6.59
MnO	0.14	0.21	0.26	0.27	0.18	0.20	0.18	0.12	0.08	0.07	0.17	0.09
MgO	7.61	6.53	9.88	7.97	4.73	4.11	4.07	3.38	3.70	3.69	7.08	1.49
CaO	11.65	9.73	9.59	8.24	11.50	6.46	2.99	7.06	6.62	6.33	11.15	4.91
Na ₂ O	3.54	2.52	2.84	2.49	2.09	2.82	3.12	2.86	3.48	3.35	2.36	4.28
K ₂ O	2.60	4.62	0.29	0.46	0.73	1.54	2.92	2.04	1.33	0.84	0.51	2.78
P ₂ O ₅	0.27	0.28	0.07	0.09	0.12	0.16	0.11	0.14	0.13	0.19	0.28	0.48
V	n/d	n/d	n/d	n/d	n/d	n/d	n/d	n/d	n/d	n/d	255	106
Cr	469	47.1	n/d	n/d	n/d	n/d	n/d	13.8	102.4	63.9	281	9
Ni	51.5	21.5	106.9	46.5	20.7	10.8	7.4	bdl	42.7	bdl	111	16
Cu	95	104.1	138.5	144.9	32	83.9	75.6	74.3	61.1	6.9	130	59
Zn	56.1	40.3	146.8	165.5	84.4	97.4	51.4	55.1	53.8	33.7	98.5	91
Rb	30.4	91.4	3.5	8.9	1.5	28.9	51.9	47.8	27.1	13.5	10.3	67.8
Sr	385	789	180	211	335	389	305	315	517	485	376	634
Y	14.8	13.2	8.1	10.8	13.2	19.7	15.8	16.9	9.2	8.6	22.7	19.4
Zr	42.3	58.3	19.9	30.2	32	104.2	116	88.8	95.6	88.9	148.3	222
Nb	1.75	2.4	0.98	1.51	1.2	2.63	2.69	3.52	3.71	3.54	16.3	13.7
Ba	158	332	259	152	16.3	149	470	209	200	167	127	1226
Hf	1.33	1.84	0.75	1.02	1.06	3.33	4.05	2.35	2.54	3.02	4.07	5.3
Ta	0.88	0.65	0.78	0.4	0.59	0.45	0.39	0.75	1.34	1.74	1.28	0.9
Th	3.01	3.77	0.37	0.58	0.70	2.53	2.61	5.03	2.91	2.37	1.07	6.6
U	1.06	1.10	0.22	0.21	0.31	0.84	0.69	1.13	0.88	0.64	0.41	1.97
La	8.80	7.95	8.72	4.17	5.68	18.18	10.96	11.40	6.68	5.14	15.40	36.63
Ce	25.63	24.47	5.68	8.98	13.04	27.08	23.11	29.43	25.27	22.93	35.60	68.80
Pr	3.27	2.90	0.78	1.22	1.75	3.48	3.23	4.06	3.11	2.66	5.08	7.87
Nd	15.73	12.77	4.25	6.26	9.38	15.80	13.17	12.60	11.00	10.82	22.7	31.97
Sm	3.53	3.05	1.02	1.74	2.39	3.41	3.12	3.08	2.34	2.39	5.80	5.71
Eu	1.13	0.92	0.50	0.47	0.71	1.15	1.43	1.15	0.83	0.65	2.10	1.59
Gd	3.99	3.06	1.27	1.58	2.21	3.22	4.52	3.27	2.70	1.93	6.25	5.43
Tb	0.37	0.40	0.22	0.26	0.44	0.54	0.54	0.40	0.21	0.20	0.87	0.74
Dy	2.89	2.66	1.84	2.14	2.67	3.61	3.12	3.29	2.10	1.48	5.34	3.60
Ho	0.55	0.54	0.43	0.48	0.61	0.83	0.82	0.69	0.39	0.33	0.98	0.70
Er	1.69	1.79	1.12	1.36	1.58	2.35	1.90	1.53	0.78	0.94	2.60	1.87
Tm	0.20	0.22	0.22	0.18	0.28	0.36	0.23	0.27	0.16	0.13	0.35	0.30
Yb	1.65	1.69	1.08	1.49	1.63	2.91	2.27	1.81	1.04	0.67	1.98	1.68
Lu	0.21	0.25	0.19	0.23	0.24	0.39	0.34	0.22	0.15	0.09	0.27	0.27
Mg#	0.76	0.74	0.82	0.79	0.67	0.66	0.69	0.50	0.58	0.58		
Ce/Yb _N	4.01	3.75	1.36	1.56	2.07	2.41	2.63	4.20	6.31	8.82		
Eu/Eu*	0.92	0.92	1.34	0.87	0.94	1.06	1.16	1.11	1.01	0.93		

Sample locations are shown in Fig. 4. $\text{Eu}/\text{Eu}^* = \text{Eu}_N / \sqrt{[(\text{Sm})_N \cdot (\text{Gd})_N]}$; $\text{Mg}\# = 100[\text{Mg}^{2+} / (\text{Mg}^{2+} + \text{Fe}^{2+})]$.

filaments, respectively, using a Finnegan MAT 262 multicollector mass spectrometer. Nd was run as the metal species on triple Ta–Re–Ta filament assemblies using a VG354 multicollector mass spectrometer. Blanks for Sr, Nd and Pb were less than 400 pg, 250 pg and 150 pg respectively. Reference standards throughout the course of analysis averaged values of $^{87}\text{Sr}/^{86}\text{Sr} = 0.710243 \pm 7$ (1σ), $n = 10$, for the NBS 987 standard, and $^{143}\text{Nd}/^{144}\text{Nd} = 0.511887 \pm 21$ (2σ), $n = 7$, for the La Jolla standard. $^{87}\text{Sr}/^{86}\text{Sr}$ was normalised

during run time to the accepted value of the international standard NBS987 = 0.71024; $^{143}\text{Nd}/^{144}\text{Nd}$ was normalised to the accepted international La Jolla standard = 0.51186. Measured values for the NBS981 standard were $^{206}\text{Pb}/^{204}\text{Pb} = 16.906 \pm 6$, $^{207}\text{Pb}/^{204}\text{Pb} = 15.447 \pm 6$ and $^{208}\text{Pb}/^{204}\text{Pb} = 36.553 \pm 18$, $n = 20$, and data were corrected to this standard.

Loss on ignition (LOI) was not part of the fusion process, so assessment was also made of the effects of alteration on samples by thin section analysis. Tables 1–4

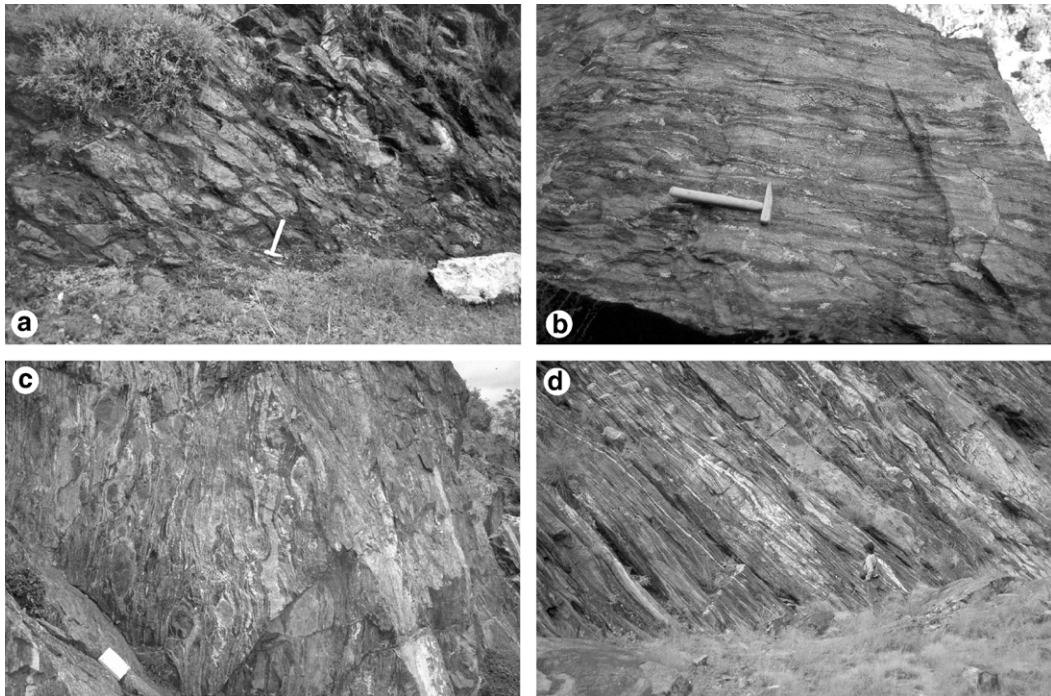


Fig. 5. (a) Deformed, pillowed lavas of the Kamila Amphibolite at Chuprial, Swat; (b) screen of deformed, pillowed, lavas of the Kamila Amphibolite enclosed in rocks of the Kohistan Batholith, Asrit, Swat; (c) deformed, pillowed lavas of the Kamila Amphibolite, Dir; (d) deformed pillowed lavas of the Gashu Confluence Formation, Jaglot Group, Thelichi.

list analyses of representative samples and international reference standards. Data for the reference materials fall within acceptable limits of less than 5% of published values for major elements, and less than 15% for trace elements. Each dataset was analysed statistically by

variance to test the null hypothesis that the means of the compared data were equal. Any samples which failed this test were rejected. All of the volcanic rocks that predated suturing to Asia have been metamorphosed to greenschist to amphibolite facies, but show little post-metamorphic

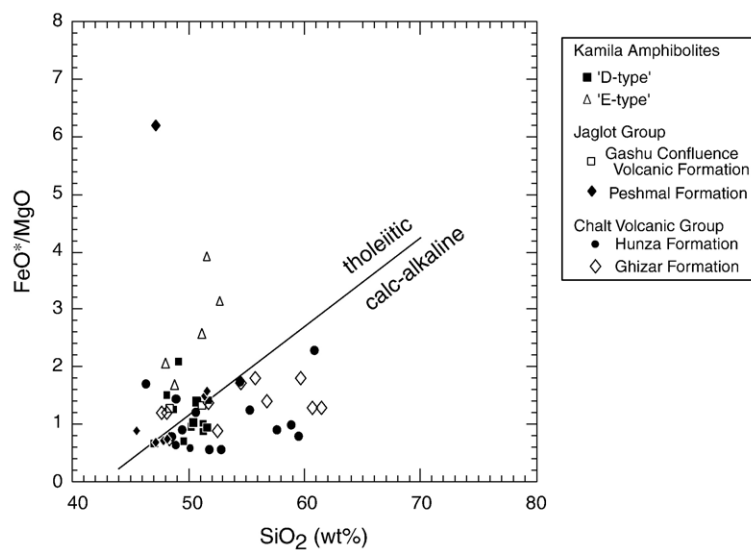


Fig. 6. Plot of FeO*/MgO against SiO₂ wt.% showing the tholeiitic and calc-alkaline associations of the rocks of the juvenile Kohistan arc (after Miyashiro, 1974).

hydration. However, because the LIL elements are highly mobile, emphasis in this study is placed on water-immobile HFSE, and the rare earth elements in particular, which have similar chemical and physical properties to each other.

3.1. Kamila Amphibolites

The Kamila Amphibolites crop out in the Swat valley, to the south of the Chilas Complex in the Swat and Indus Valleys and to both north and south of the

Chilas Complex in the Dir Valley (Figs. 1–3). Within, and to the east of, the Indus Valley the state of deformation is such that no primary features are preserved (Treloar et al., 1990). Pillow lavas are preserved to the west of the Indus Valley, in the Swat and Dir Valleys. The pillows have fine-grained rims, which represent metamorphosed chilled margins, and are 20–30 cm in length, decreasing in size toward the south of the outcrop (Fig. 5a). Deformed tonalites of the Stage 1 Kohistan Batholith at Asrit (Fig. 2) enclose screens of pillowed metavolcanic rocks of the Kamila

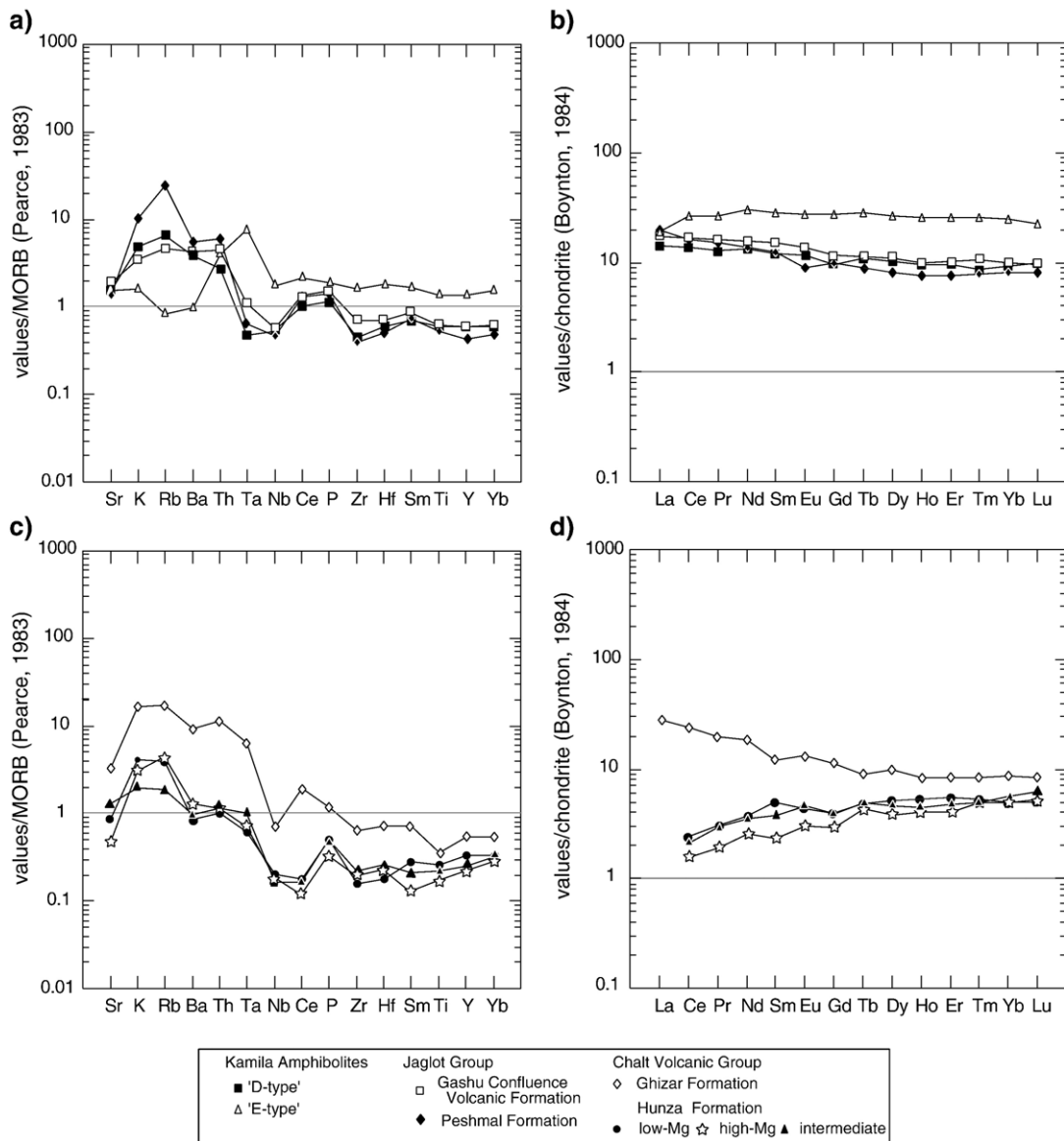


Fig. 7. Multi-element and rare earth element diagrams, comparing mean values of the metavolcanic basic rocks of: (a, b) the Kamila Amphibolites ('E-type', $n=5$; 'D-type', $n=11$, Jaglot Group (Gashu Confluence Volcanic Formation, $n=2$, Peshmal Formation, $n=7$); and (c, d) Chalt Volcanic Group (Ghizar Formation, $n=4$; Hunza Formation, low-Mg, $n=4$, high-Mg, $n=7$, intermediate, $n=4$).

Amphibolite sequence (Fig. 5b). These xenoliths are deformed, fine-grained, layered epiclastic tuffs which are rich in hornblende. In the southern part of the Dir section near Timagora (Fig. 3), the Kamila Amphibolites are intruded by gabbro-norites of the Chilas Complex and by granodiorite sheets of the Kohistan Batholith. As in Swat, the volcanic rocks are extensively pillowed (Fig. 5c), but here they are flattened and elongated due to deformation.

Khan et al. (1993) divided the Kamila Amphibolites into two suites based on their geochemistry. One group (the high-Ti or ‘E-type’ series) is enriched in TiO_2 (1.69–2.24%), high field strength elements (HFSE), and heavy rare earth elements (HREE). The other group (the low-Ti or ‘D-type’ series) is relatively depleted in TiO_2 (0.57–1.36%), HFSE, and HREE. Treloar et al. (1996) noted that the ‘E-type’ series has geochemical similarities with the Ontong–Java plateau, in particular the flat REE and HFSE patterns and the lack of Ta–Nb negative anomalies. They thus interpreted it as the intraoceanic crust on which the arc was built. The ‘D-type’ series has a distinct negative Nb anomaly and the geochemical characteristics of a subduction-related arc, and thus contains the earliest arc-related rocks of Kohistan. In accordance with Khan et al. (1993), the enriched group is referred to here as the ‘E-type’ group, and the depleted group as ‘D-type’.

Analytical data for the Kamila Amphibolites are listed in Table 1. For those samples prefixed with ‘A’, the major element, Pb and isotope data are taken from Khan et al. (1997). The high-Ti, ‘E’-type, samples are all tholeiitic. The ‘D’-type samples span the tholeiitic/calc-

alkaline divide on a plot of SiO_2 vs. FeO^*/MgO (Fig. 6). Two samples have high Mg# (DR16=0.73; SW2=0.4). Two fine-grained, foliated and homogeneous samples collected from the Niat valley in E. Kohistan (002 and 001) are analysed here. The rocks have TiO_2 contents of 2.19% and 2.20% and compare well with the high-Ti ‘E-type’ group of Khan et al. (1993). The ‘E-type’ rocks (Fig. 7a) display variable light ion lithophile element (LILE) concentrations, although the normalised $(\text{Nb}/\text{Yb})_{\text{N}}$ HFSE ratios are close to 1. There are no negative Nb anomalies. The REE pattern for the ‘E-type’ samples (Fig. 7b) is flat. Mean $(\text{Ce}/\text{Yb})_{\text{N}}$ ratios are 1.1. Element concentrations are 20–30 times chondritic values. The multi-element pattern for the ‘D-type’ rocks (Fig. 7a) shows a distinct negative Nb anomaly, and a greater enrichment in the LILE than is shown by the ‘E-type’ rocks. The rare earth element diagram (Fig. 7b) shows element concentrations of about 10 times chondrite values. There is some slight enrichment in the LREE, with $(\text{Ce}/\text{Yb})_{\text{N}}$ ratios averaging 1.8 and Eu anomalies averaging 1.0. $^{87}\text{Sr}/^{86}\text{Sr}$ (0.70446) and $^{143}\text{Nd}/^{144}\text{Nd}$ (0.51274; $\epsilon\text{Nd}_{120}=2.19$) ratios are in the range reported by Khan et al. (1997) and Bignold and Treloar (2003).

The trace element patterns for the ‘D-type’ and ‘E-type’ Kamila Amphibolites are significantly different (Fig. 7a). The ‘E-type’ pattern is only slightly enriched relative to MORB and has no negative Nb anomaly. Conversely, the ‘D-type’ pattern is enriched in the LILE relative to MORB and has a clear negative Nb anomaly. These differences are reflected in the REE patterns (Fig. 7b) where the ‘E-type’ Kamila Amphibolites have a flat pattern and an enrichment of

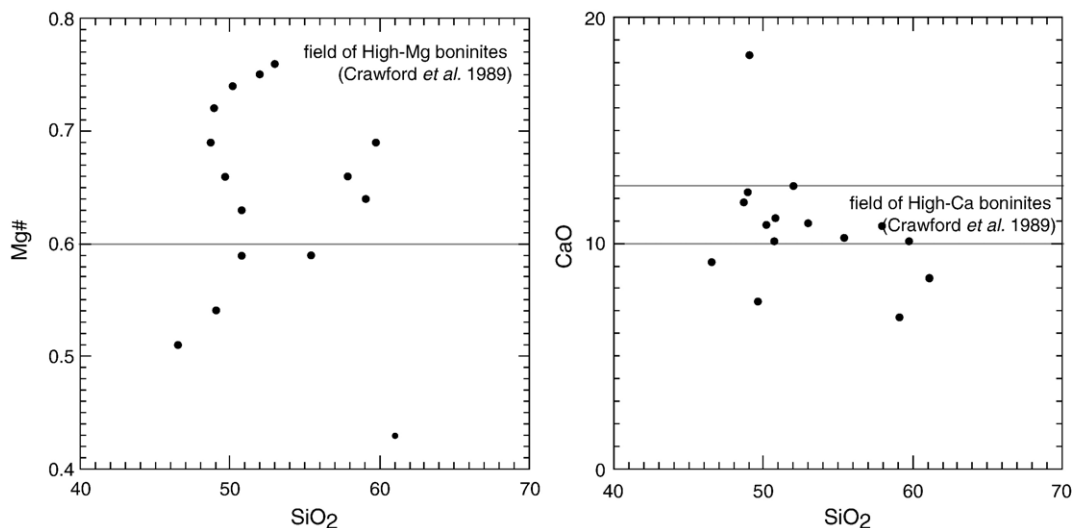


Fig. 8. Plots of (a) Mg# and (b) CaO vs. SiO_2 for samples from the Chalt Volcanic Group Hunza Formation.

about 20 times chondrite values, although with slight depletions in the LREE and in Lu relative to the other REE. The ‘D-type’ Kamila Amphibolites are enriched by about 10 times chondrite values with a slight enrichment in the LREE relative to the HREE. Lu is also slightly enriched relative to Yb.

3.2. Jaglot Group

The Jaglot Group comprises sequences of basalts and andesites, interbedded with sedimentary rocks, with variable volcanoclastic contents. All have been metamorphosed to greenschist or lower amphibolite facies.

3.2.1. Gashu Confluence Volcanic Formation

The Jaglot Group in the Indus Valley is subdivided into three formations Khan et al. (1994). The Gilgit Formation comprises mainly paragneisses and schists of sedimentary origin, and has a transitional contact with the overlying Gashu Confluence Volcanic Formation (Khan et al., 1994, 1996). The Gashu Confluence Volcanic Formation is a suite of north-dipping, flattened and sheared, pillowed, lavas, mafic sills and tuffs, which crop out to the north of Thelichi (Fig. 1). The pillows are set in a fine-grained, finely laminated matrix and are more abundant toward the southern end of the outcrop (Fig. 5d). They are variably coloured, ranging from dark

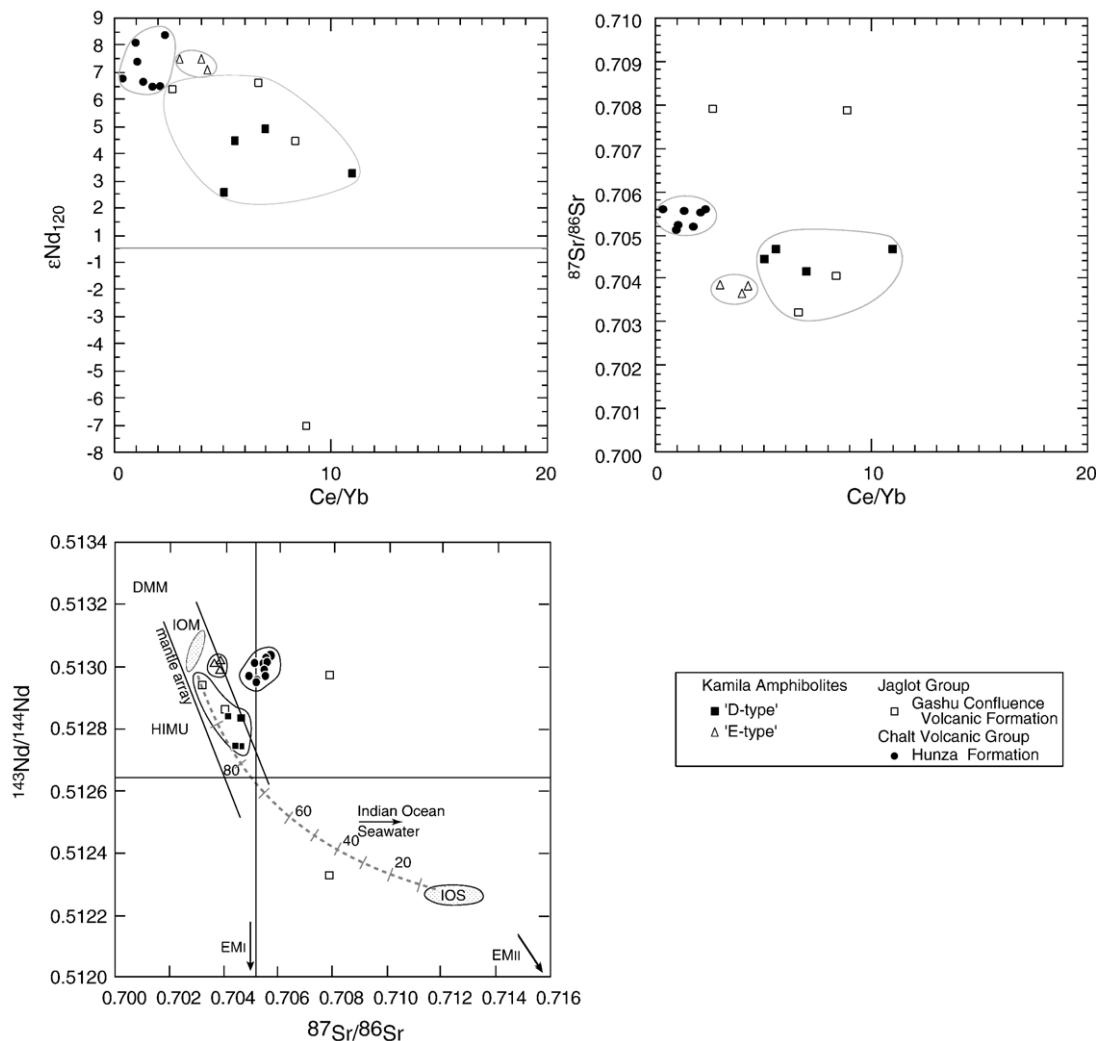


Fig. 9. Plots of (a) ϵNd_{120} , (b) $^{87}Sr/^{86}Sr$ vs. Ce/Yb and (c) $^{143}Nd/^{144}Nd$ vs. $^{87}Sr/^{86}Sr$ for selected igneous rocks of the Kohistan island arc. IOS = Indian Ocean sediments, IOM = Indian Ocean mantle, DMM = depleted MORB mantle. Calculations of ϵNd_{120} are in accordance with Khan et al. (1997). Outlying samples are interpreted as containing an enhanced contribution from a sedimentary source (Bignold and Treloar, 2003).

green to cream. Their thickness varies between 4 and 40 cm. The sills have experienced intense stretching and thinning, and are boudinaged giving the appearance of being pillowed, but the glassy chilled rims typical of pillows are not present. The tuffs contain deformed air fall lapilli. Hornblende gabbro crystals overprint the fabric and may postdate deformation.

Near Thelichi the Jaglot Formation rocks are folded by the large amplitude Jaglot synform (Coward et al., 1987). Within the synform, the Gashu Confluence Volcanic Formation passes upward into a sequence of slates and sandstones overlain by marbles interbedded with mafic tuffs and sills, in turn overlain by slates and sandstones. These rocks, which occupy the core of the Jaglot syncline, are part of the Thelichi Formation, the uppermost unit of the Jaglot Group.

Basalts and andesites of the Gashu Confluence Volcanic Formation have Mg# ranging between 0.39 and 0.64, and >6.0 wt.% MgO (Fig. 6a). The basalts have >1.0 wt.% TiO₂, and low Cr and Ni contents (Table 2). On a multi-element diagram, the Gashu Confluence Volcanic Formation rocks have a clear subduction-related chemical signature, the HFSE being slightly depleted relative to MORB, but with similar values to the Kamila Amphibolites (Fig. 7a). The rare earth element pattern has a similar slope to that of the 'D-type' Kamila Amphibolites with a mean (Ce/Yb)_N ratio of 1.9, and is slightly more enriched in the LREE relative to the chondrite standard (Fig. 7b). ⁸⁷Sr/⁸⁶Sr ratios range between 0.70323 and 0.70791, and ¹⁴³Nd/¹⁴⁴Nd ratios between 0.51230 and 0.51297 (εNd₁₂₀: –6.93 to 6.44) (Bignold and Treloar, 2003).

3.2.2. Peshmal Formation

In the Dir District, the N-dipping rocks of the Kamila Amphibolite Belt pass upward into the Peshmal Formation. A traverse along the Karandokai Khwar, a tributary flowing eastward into the Swat River south of Kalam (Fig. 2), provides the type section through the Peshmal Formation. The rocks, which dip gently to the northwest, are mostly layered biotite psammites and pelites, some garnet-bearing, and resemble the layered Gilgit Paragneisses which crop out in the east of the arc. They contain variable amounts of hornblende. Finely bedded layers are often crenulated, sheared and intensely folded. Thin calc-silicate bands and lenses are also present. Interbedded volcanic horizons are generally mafic. They are thin, mostly <4 cm, often boudinaged, and contain abundant garnet and hornblende. There is a higher proportion of metasedimentary rocks to metavolcanic rocks than in the Indus Valley. The basalts of the Peshmal Formation are tholeiitic and calc-alkaline in type (Fig. 6a). On a multi-

element diagram, the HFSE are slightly depleted with respect to MORB and enriched in the LILE. The slightly irregular pattern shown by the LILE may reflect element mobility during either or both, of metamorphism and subsequent hydration. The rocks have low TiO₂ contents (Table 2) and pronounced negative Nb anomalies (Fig. 7a). The rare earth element patterns (Fig. 7b) show a slight enrichment in LREE relative to HREE, with mean (Ce/Yb)_N ratios of 2.3 in Swat and 2.0 in Dir. There are small negative Eu anomalies in the rocks, those from Swat averaging 0.7 and those from Dir, 0.9. Both the HFSE and REE patterns are similar to those of the 'D-type' Kamila Amphibolites, but are slightly more depleted than those of the Gashu Confluence Volcanic Formation.

Although the mean data show similar trends on multi-element and REE plots, basaltic samples from the GCV of the Jaglot Group are chemically distinct from those of the Peshmal Formation with which they are correlated, with only sample (TL5) being similar. The Peshmal Formation, which crops out between 200 and 300 km to the west of the GCV, has been metamorphosed to greenschist rather than amphibolite facies, and shows more post-metamorphic alteration, and this might explain the differences in the LILE. The LREE/HREE ratios (Ce/Yb)_N are greater in the Peshmal Formation than the Gashu Confluence Volcanic Formation. The latter also shows depletion in normalised Lu, not seen in the Peshmal Formation. The LREE of the Peshmal Formation is enriched, and the HREE depleted, relative to the 'D-type' Kamila Amphibolites.

3.3. Chalt Volcanic Group

The Chalt Volcanic Group (CVG) overlies the Jaglot Group to the south and is overlain by the Yasin Group to the north. Where the Yasin Group is absent, the CVG lies in direct contact with the Shyok Suture Zone. The CVG is divided into two Formations on the basis of chemical and lithological variations (Pettersen et al., 1990; Pettersen and Windley, 1991; Pettersen and Treloar, 2004). The Hunza Formation crops out in the east and the Ghizar Formation in the west.

3.3.1. Hunza Formation

The type section of the Hunza Formation is exposed along the Karakoram Highway in the Hunza Valley, where it passes upward into the Yasin Group (Figs. 1, 4). This section has been described in detail by Robertson and Collins (2002) and Pettersen and Treloar (2004). The volcanic rocks comprise massive flows, some pillowed, epiclastic tuffs and ignimbritic flows. Although most of the rocks have a steep

southward dip, there is evidence, from inverted slump structures and grain sizes fining downward in tuffaceous material, that the sequence is overturned, and that the rocks young northward. Rare felsic rocks contain randomly orientated hornblende needles. The Hunza Formation is intruded, along its southern margin, by rocks of the Kohistan Batholith.

Rocks of the Hunza Formation are mainly calc-alkaline in nature (Pettersen and Windley, 1991; Table 3; Fig. 6). They show a range in Mg contents from high-Mg (9–15 wt.%) basalts and andesites to low-Mg basalts, andesites and minor rhyolites. The major element chemistry of these rocks has been described by Pettersen and Windley (1991), and only the trace element chemistry is described here. Pettersen and Windley (1991) grouped the basic and intermediate rocks into a low-silica type, which also has low Mg content (<9% MgO, Mg# 0.51–0.59, here called the low-Mg type), and a high-Mg type. High-Mg intermediate rocks with SiO₂ contents of 52–61% also have >11% MgO, Mg# 0.69–0.76 (Fig. 8a). The multi-element patterns (Fig. 7c) show that both groups have negative Nb anomalies and have HFSE values strongly depleted with respect to MORB. These anomalies are masked by the low Ce concentrations typical of these rocks. The rare earth element patterns for all the basic and intermediate samples (Fig. 7d) show an unusual positive slope, which is most pronounced in the most basic rocks. The depletion in the LREE relative to the HREE indicates depletion in clinopyroxene and orthopyroxene in the source region. Mean (Ce/Yb)_N ratios for the high-Mg suite are 0.3, and Eu anomalies are negligible. The REE patterns for the low-Mg group (Fig. 7d) vary from positive slopes to flat, with mean (Ce/Yb)_N ratios of 0.7.

The intermediate rocks which are not included in the high-Mg group show patterns similar to, but slightly more enriched than, those of the high-Mg group in the multi-element diagram (Fig. 7c). The rare earth element pattern is similar to that of the low-Mg group, both being slightly enriched in the LREE in comparison with the high-Mg group. The mean (Ce/Yb)_N ratio is 0.4, and mean Eu anomaly is 1.3.

⁸⁷Sr/⁸⁶Sr ratios range between 0.70514 and 0.70559, and ¹⁴³Nd/¹⁴⁴Nd ratios range between 0.51296 and 0.51301 (Bignold and Treloar, 2003). All are in the range reported by Khan et al. (1997).

Some of the rocks of the Hunza Formation high-Mg group were identified by Pettersen et al. (1990) and Pettersen and Windley (1991) as having the general geochemical characteristics of boninites as defined by Cameron et al. (1979) and Gill (1981). SiO₂ content of

the rocks is 51–56 wt.%, MgO > 6 wt.% (Mg# 0.51–0.76), Cr > 500 ppm, Ni > 100 ppm, low TiO₂ (<0.4–0.5 wt.%), with low concentrations of P, Zr and REE. Of the seventeen rocks analysed by Pettersen and Windley (1991), eight satisfied these criteria. On the basis that the samples contain 10–12.5% CaO (Fig. 8), Khan et al. (1997) further described them as high-Ca boninites, generally considered to occur in fore-arc regions (e.g., Crawford et al., 1989; Bloomer et al., 1995). However, a description as high-Mg rocks with boninitic affinities is preferred here since, although these rocks clearly have some of the chemical pre-requisites for boninites, not all the requirements are fulfilled.

3.3.2. Ghizar Formation

The field relationships of the rocks of the Ghizar Formation are fully described by Pettersen and Treloar (2004). Basalts and andesites are tholeiitic to calc-alkaline, the majority being calc-alkaline (Fig. 6a). Mg numbers range between 0.49 and 0.7 (Table 4). The multi-element pattern (Fig. 7c) shows a negative Nb anomaly, consistent with island arc volcanic rock and the HFSE show a restricted range of concentrations between typical tholeiitic and primitive MORB (Pearce, 1983). This pattern is similar to those of the ‘D-type’ Kamila Amphibolites and the Jaglot Group (Fig. 7a). The rare earth element pattern for the Ghizar Formation (Fig. 7d) is more enriched in the LREE than those of the ‘D-type’ Kamila Amphibolites and the Jaglot Group, with a mean (Ce/Yb)_N ratio of 2.92.

The geochemistry of the Hunza Formation clearly defines it as a different group from the Ghizar Formation and confirms the division of the Chalt Volcanic Group into two. The multi-element and REE patterns from the Ghizar Formation are within the range of the ‘D-type’ Kamila Amphibolites and the Jaglot Group (Fig. 7a, c), which have typical arc-related signatures. The HFSE of the Hunza Formation plot below the level of primitive MORB (Pearce, 1983) (Fig. 7c), the REE patterns show depletion in the LREE compared with enrichment in the Ghizar Formation (Fig. 7d), and are depleted in the HREE relative to the ‘D-type’ Kamila Amphibolites, the Jaglot Group and the Ghizar Formation.

3.4. Summary of the geochemical variations in the volcanic rocks of the Kohistan island arc

Geochemical and isotopic data from Tables 1–4, Figs. 7 and 9 clearly define three different magmatic successions within the juvenile arc. The chemically distinctive ‘E-type’ Kamila Amphibolites form one succession. These are enriched in the HFSE and REE represent pre-

subduction ocean floor basalts. The ‘D-type’ Kamila Amphibolites, the Jaglot Group and the Ghizar Formation of the Chalt Volcanic Group form the second succession. These are all chemically similar in their HFSE and REE patterns, and show a clear arc volcanic signature (c.f., Pearce, 1983). The Hunza Formation of the Chalt Volcanic Group, with its high-Mg basalts and andesites, clearly represents a different magmatic source from the main arc volcanic rocks. High-Mg basalts and andesites are commonly found in fore-arc settings and are increasingly being reported from back-arc regions (Falloon et al., 1992; Meffre et al., 1996). The Hunza Formation is the youngest succession of the Kohistan arc, and lies at the same stratigraphic level as the Ghizar Formation. With its depletion in the HFSE and the LREE, its weak arc signature and high-Mg rocks which require a source with high heat flow, this succession represents the formation of a back-arc spreading centre (Bignold and Treloar, 2003).

4. Rare earth element modelling of rocks of the juvenile arc

The rare earth elements have similar chemical and physical properties but, because of small differences in ionic radius, they may become fractionated relative to each other. As a result, they are particularly useful for modelling mantle melting in order to try to identify appropriate mantle sources for the rock suites and the types and amounts of partial melting that may have been involved.

Rare earth element modelling in this study was carried out using computer software ‘DW’, developed by David Woodhead of Liverpool University, and was based on equations for batch and fractional partial

melting (Wood and Fraser, 1986). Modelling takes the REE composition of a source region and calculates the REE composition of rocks resulting from varying percentages of partial melting. This process takes into account the mineralogy of the source, the percentage of each of the minerals that enter the melt and their partition coefficients. This may be taken a step further by comparing results with known compositions of rock suites. In this way a source region for these rocks may be identified when calculated REE concentrations of a melt, at a given percentage of partial melting, replicate or fall close to these known values. The partition coefficients used in this study are listed in Table 5.

The Kohistan rocks have been metamorphosed to greenschist and amphibolite facies, and their initial igneous mineralogy is therefore unknown. The samples from the Dir region in particular have been hydrated after metamorphism and only the least altered have been used in this study. The only known factor is the end product — voluminous basalts that we infer, on the basis of the isotope data, have little crustal contamination and no evidence for significant fractionation in a sub-surface magma chamber. Therefore, the modelling ignores the potential effects of fractionation and considers solely batch/equilibrium melting of a mantle source. The similarity of the trace element patterns and REE curves (Fig. 7) shows element mobility in the LIL elements but not in the high field strength elements or the REE. Therefore, although the initial mineralogy of the rocks is unknown, during metamorphism the REE chemistry of rocks remains essentially the same.

Certain assumptions have had to be made in order to model mantle sources for the Kohistan rocks. REE analyses have been taken from the literature in order to

Table 5
Partition coefficients used in rare earth element modelling (Hanson, 1980) B/A = basaltic andesite

	Hornblende (B/A)	Clinopyroxene (mantle)	Orthopyroxene (mantle)	Olivine (mantle)	Garnet (mantle)	Spinel (mantle)	Plagioclase (B/A)	Plagioclase (mantle)
La	0.06	0.054	0.002	0.0004	0.01	0.01	0.02	0.27
Ce	0.09	0.098	0.003	0.0005	0.021	0.01	0.02	0.20
Pr		0.15	0.005	0.0008	0.054			0.17
Nd	0.16	0.21	0.0068	0.001	0.087	0.01	0.02	0.14
Sm	0.24	0.26	0.01	0.0013	0.217	0.01	0.02	0.11
Eu	0.26	0.31	0.013	0.0016	0.32	0.01	2.10	0.73
Gd	1.10	0.30	0.016	0.0015	0.498	0.01	0.02	0.066
Tb	1.10	0.31	0.019	0.0015	0.75	0.01	0.02	0.06
Dy	1.00	0.33	0.022	0.0017	1.06	0.01	0.01	0.055
Ho		0.31	0.026	0.0016	1.53			0.048
Er	1.00	0.30	0.03	0.0015	2.00	0.01	0.01	0.041
Tm		0.29	0.04	0.0015	3.00	0.01		0.036
Yb	1.00	0.28	0.049	0.0015	4.03	0.01	0.006	0.031
Lu	0.82	0.10	0.06	0.002	5.50	0.01	0.006	0.025

model potential mantle sources. Selection of an appropriate mantle source, mineralogy and chemistry is not easy. The modelling process is extremely sensitive, so that unrealistic estimates of chemistry and mineralogy of the source and of melt proportions will produce results that do not match the chemistry of the known end product. Hence, given the end products, it is possible to exclude a number of sources as, regardless of source mineralogy and melt proportion, they never produce a melt chemistry similar to that of the real rock. There is a limited number of REE analyses of mantle rocks, and there is no evidence that the present-day Indian Ocean mantle is the same as Neotethyan mantle (Mahoney et al., 1998). Potential mantle sources tested included primitive mantle (McDonough et al., 1992; McDonough and Sun, 1995), C1 chondrite, N-MORB, and E-MORB (Sun and McDonough, 1989), and estimates were made of the mineralogy of these source regions and the extent of batch or fractional partial melting of the minerals in them. Of these, only the values of McDonough et al. (1992) produced melts with chemistries similar to those of the Kohistan rocks.

Because this is a modelling exercise, and some rock suites contain only a small number of samples, the results presented here can be used only as an indicator of the source region and of the petrogenetic processes that might have taken place in the mantle during extraction of the arc magmas. Where similar results were obtained for both batch and fractional partial melting, the models were analysed statistically for comparison with the relevant rock suite, and only the closest fit for each model is presented. In the event, only models of batch partial melting yielded the best results. All results are presented in REE diagrams normalised against chondrite (Boynnton, 1984).

4.1. Kamila Amphibolites

The REE chemistry of the ‘E-type’ and ‘D-type’ mafic rocks of the Kamila Amphibolites can both be successfully modelled using the primitive mantle concentrations of McDonough et al. (1992) as a mantle-type source. The ‘E-type’ suite can be modelled by 6% batch partial melting (Fig. 10a) and, depletion of the source in hornblende and the pyroxenes is indicated, although it was not possible to obtain a perfect match in the modelled pattern, especially in the LREE. Theoretically, the presence of garnet in the source should produce depletion in Lu. However, modelling the melting of a garnet-bearing protolith did not provide a melt of a suitable composition. A near-perfect match of the REE pattern of the ‘D-type’ suite can be modelled through

15.5% batch partial melting of a primitive mantle source that includes spinel (Fig. 10b).

4.2. Jaglot Group

Modelling of the REE chemistry of the Jaglot Group strongly suggests that the primitive mantle composition of McDonough et al. (1992) was the source, although with garnet present. Although the two rock suites of the Jaglot Group are separated by 700 km, the modelled mineralogy of the source region is constant in olivine and garnet content and differs only minimally in hornblende and pyroxene content. Batch partial melting (7.5%) of this mantle source could produce a melt with REE chemistry similar to that of the mafic rocks of the Gashu Confluence Volcanic Formation (Fig. 10c), and 13% batch partial melting a melt with an REE pattern similar to that of the mafic rocks of the Peshmal Formation (Fig. 10d).

4.3. Chalt Volcanic Group

4.3.1. Ghizar Formation

The Ghizar Formation crops out along the length of northern Kohistan to the west of the Hunza Formation. Modelling shows that the mafic rocks from the Ghizar Formation could have been generated by 4.5% batch partial melting of the primitive mantle-type of McDonough et al. (1992) (Fig. 10e).

4.3.2. Hunza Formation

In contrast to all the main arc volcanic rocks of Kohistan, the mafic rocks of the Hunza Formation are significantly depleted in the LREE, with a mean (Ce/Yb)_N ratio of 0.3. These rocks require an LREE-depleted source. No REE analyses are available for the ultramafic rocks of southern Kohistan, and the eastern side of Ladakh is thought to be founded on continental basement (Rolland et al., 2000). Therefore, analyses from the literature of other LREE-depleted rocks were used for modelling the Hunza Formation. These included dunite from Ladakh (Rolland et al., 2000), Alpine spinel lherzolite (Loubet et al., 1975), N-MORB (Sun and McDonough, 1989) and Ronda spinel lherzolite (Frey et al., 1985). From these, successful modelling was only possible using the depleted spinel lherzolite REE data of Loubet et al. (1975). Fig. 11a–c shows that these Mg-rich, LREE-depleted basalts must have been extracted through batch partial melting of a mantle source with chemistry close to that of this starting material. REE concentrations from this source are only slightly more

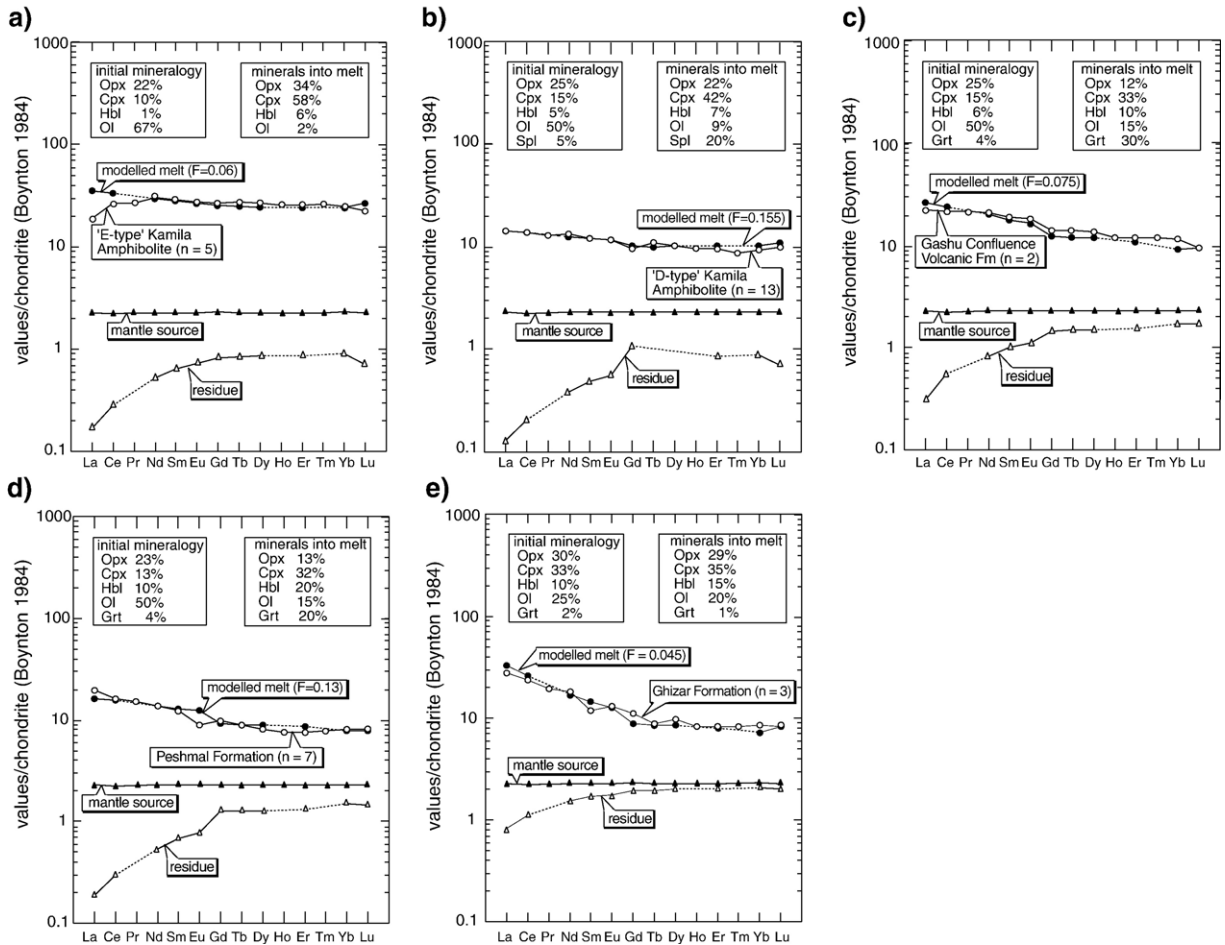


Fig. 10. Mantle melting models for rocks of the Kohistan island arc generated from batch partial melting of a mantle source type similar to calculated primitive mantle (McDonough et al., 1992). (a) 'E-type' Kamila Amphibolites: REE concentrations of the residue are similar to those of depleted spinel lherzolite xenoliths from the European Alps (Loubet et al., 1975); (b) 'D-type' Kamila Amphibolites; (c) Jaglot Group, Gashu Confluence Volcanic Formation; (d) Jaglot Group, Peshmal Formation; (e) Chalt Volcanic Group, Ghizar Formation. F = melt fraction, mantle.

enriched than those of the mantle residue calculated after the extraction of the Kamila Amphibolite 'E-type' suite (Fig. 10a). Further modelling was therefore attempted using both sets of REE concentrations as potential mantle-type sources (Fig. 11d–f). Cumulate rocks occur at the southern edge of the Kohistan arc as the Jijal, Sapat and Tora Tigga complexes (Fig. 1). These may be a small remnant of a much larger mass of intrusive cumulates, most of which were removed by delamination as a result of density instabilities and viscously removed during the duration of arc magmatism (Kelemen et al., 2003). There are no REE analyses of these rocks, and it is assumed that they would not have been a potential source.

REE modelling using depleted spinel lherzolite (Loubet et al., 1975) shows that it is possible to produce a melt through, 15.5% batch partial melting, which has a

close match to the low-Mg rocks (Fig. 11a). The match with the high-Mg and intermediate rocks is less satisfactory. Here, generation of the high-Mg rocks requires 18.5% batch partial melting (Fig. 11b) and 6% more clinopyroxene in the melt than does production of the low-Mg rocks. 15.2% batch partial melting from the same mantle source type to generate a melt similar to the intermediate rocks (Fig. 11c) requires a lower hornblende and pyroxene content, but produces similar proportions of minerals in the melt as for the low-Mg and high-Mg suites.

Batch partial melting (10%) of the residue similar to that remaining after the extraction of 'E-type' Kamila Amphibolites from a primitive mantle source type (Fig. 10a) generated basalts which matched closely those of the low-Mg suite (Fig. 11d). Similarly, 12% batch partial melting produced a match close to the

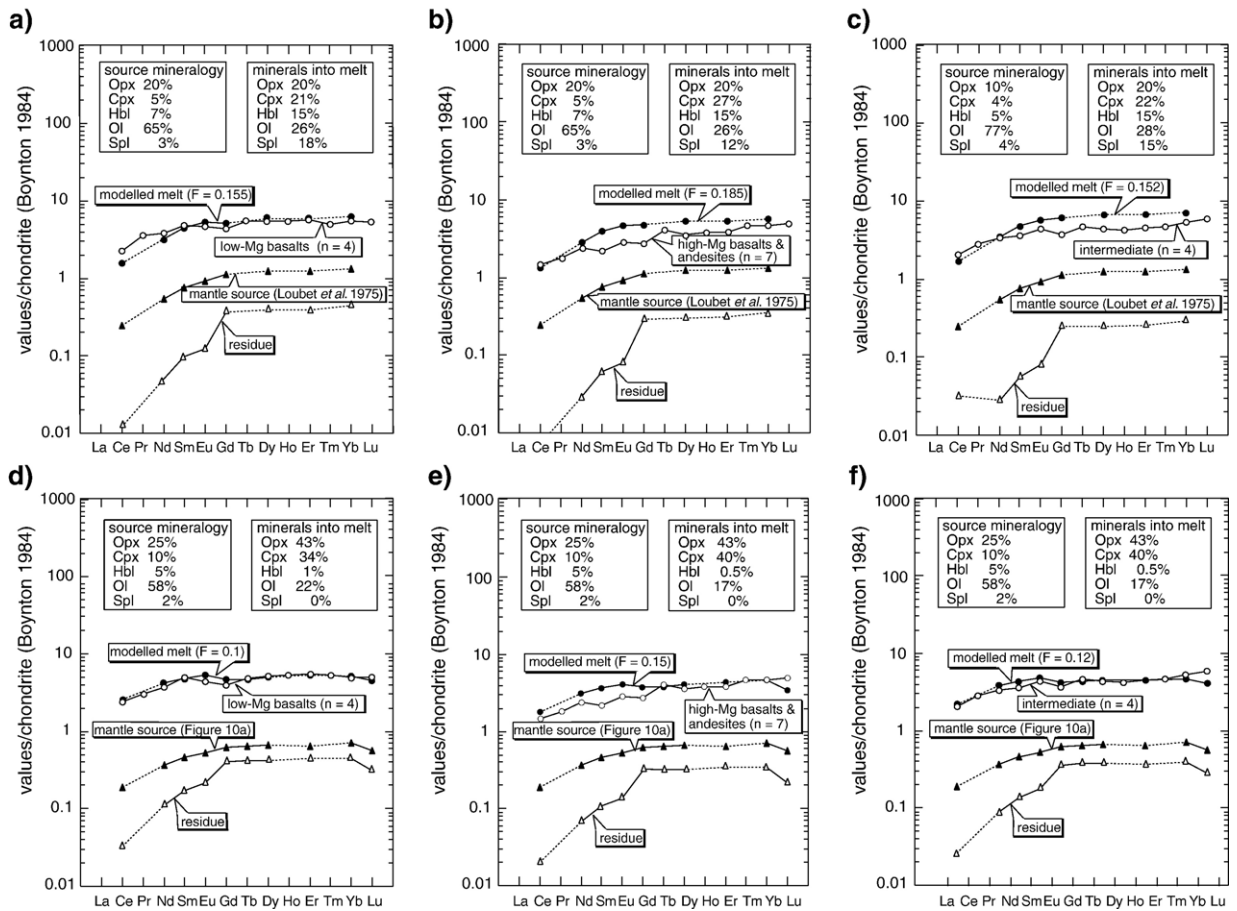


Fig. 11. Mantle melting models for rocks of the Chalt Volcanic Group, Hunza Formation, generated from (a, b, c) batch partial melting of a mantle source type with similar mineralogy and REE concentrations to depleted spinel lherzolite xenoliths from the European Alps (Loubet et al., 1975) and; (d, e, f) from the residue remaining after the extraction of the ‘E-type’ Kamila Amphibolites (Fig. 10a).

REE concentrations of the intermediate rocks (Fig. 11f). Modelling of 15% batch partial melting resulted in a less satisfactory match with the high-Mg suite (Fig. 10e), but better in the HREE than in Fig. 10b. The mineralogy used in all the models was consistent with this source being more pyroxene-enriched than depleted spinel lherzolite (Loubet et al., 1975). The high-Mg suite is formed of basalts and andesites. Andesites form as the result of remelting of underplated basalts which are contaminated by upper crustal material during their passage to the surface (Hickey and Frey, 1982; Kempton et al., 1995; Michel et al., 1999; Riley et al., 2001). Boninites are considered to be unusual forms of andesite, as their common occurrence in fore-arc settings with high heat flow indicates that they must have been generated from mantle sources. That the rocks of the Hunza Formation can be modelled from remelting of the depleted residue of a primitive mantle source would be

consistent with the possibility that high-Mg basalts and andesites can be erupted in both fore-arc and back-arc settings.

It is clear from the geochemistry and REE modelling that the mafic and intermediate rocks of the Chalt Volcanic Group were derived from two quite different mantle source types. The Ghizar Formation rocks can be best modelled from a fertile, primitive, mantle source type. Conversely, the Hunza Formation, with its characteristic depletion in the LREE, can be modelled only from a depleted mantle source. The best match comes from partial melting of a source similar to the residue of previously extracted ‘E-type’, MORB-like, Kamila Amphibolites.

5. Discussion

REE modelling presented here strongly suggests that, with the exception of the Hunza Formation, each of the

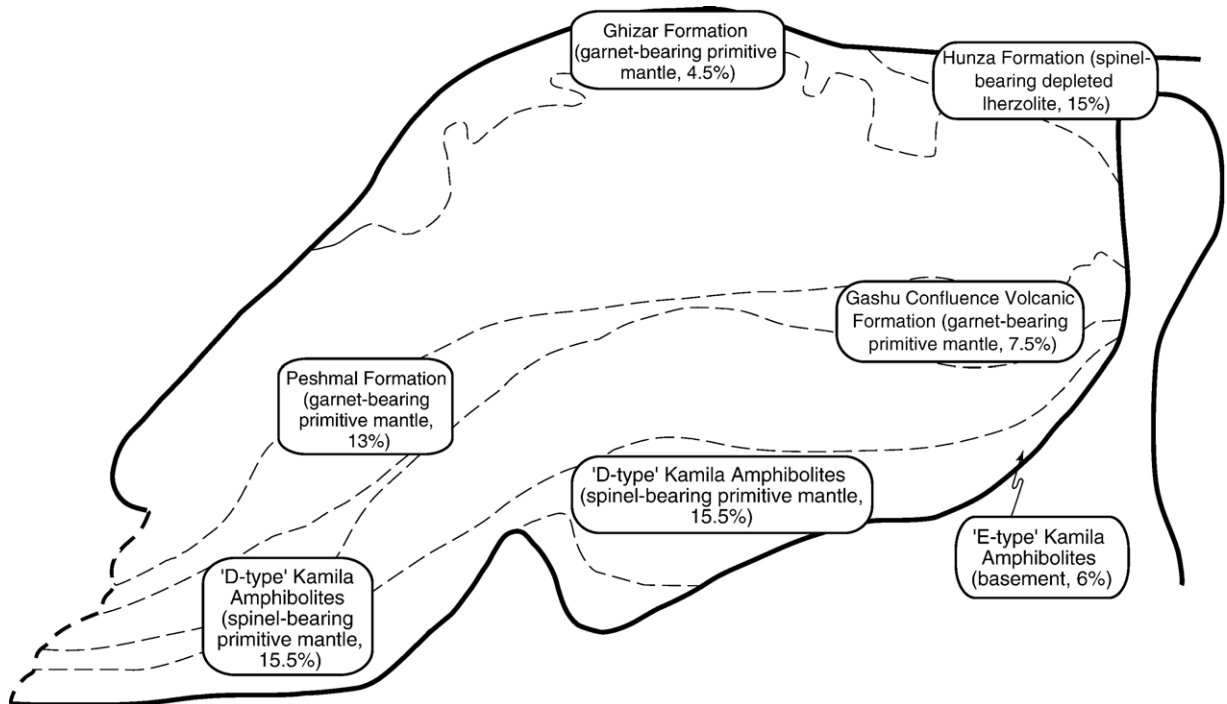


Fig. 12. Simplified geological map of Kohistan summarising the results of rare earth element modelling of the volcanic rocks of the juvenile arc. Mantle source type and degrees of partial melting (%) are indicated in brackets.

discrete volcanic sequences within the Kohistan Island Arc was derived from melting of a primitive mantle source beneath Kohistan. Modelling of the chemical data suggests significant variations in both amount and depth of melting. The latter is essentially characterised by the presence of garnet or spinel in the source. Fig. 12 shows the geographical distribution of the melt products and highlights both the mineralogy of the source and the extent of melting of that source. If the Hunza Formation is excluded, then it is clear from this figure that the amount of partial melting decreases northward and that the mineralogy of the source changes northward.

The changes through time in the modelled source region result from small, but significant, changes in basalt composition during early stages of evolution of the juvenile arc. The change from a spinel- to a garnet-bearing source documents the progressive descent of the northward subducting slab. It also suggests that the melt region was located just above the subducting slab. The isotopic data suggest that the signature is a function of fluids derived from subduction and dehydration of sea-floor sediments (Bignold and Treloar, 2003). The reduced amount of melting indicated by the modelling may also indicate that volatile release was not constant during subduction. Volatile release presumably decreases with depth as the hydrous phases in the subducting slab break down

at relatively low pressures. The result is that there is a greater volatile flux into the spinel-bearing mantle wedge than into the deeper garnet-bearing segment of the wedge.

Fig. 13 shows a model for the evolution of the volcanic rocks of the juvenile stages of the island arc. The model is underpinned by the assumption that subduction of Tethyan oceanic crust beneath the arc was to the north, as is accepted by most workers in the region (see discussion in Bignold and Treloar, 2003). It is primarily based on the recognition that three different chemical signatures are present within volcanic rocks extruded prior to suturing with Asia. Firstly, basaltic volcanic rocks of the 'D-type' Kamila Amphibolites, the Jaglot Group and the Ghizar Formation all have typical arc-type signatures, although with subtly different chemistries that result from their derivation from different source regions. Secondly, the 'E-type' Kamila Amphibolites have an enriched MORB-type signature. Thirdly, basaltic and andesitic volcanic rocks of the Hunza Formation have a very distinctive chemistry with strong depletion in the LREE.

The 'E-type' Kamila Amphibolites have REE concentrations similar to E-MORB with no arc signature. It has been demonstrated here that these rocks may have been generated in an intraoceanic setting (Fig. 13a) by 6% partial melting of a primitive mantle-type source

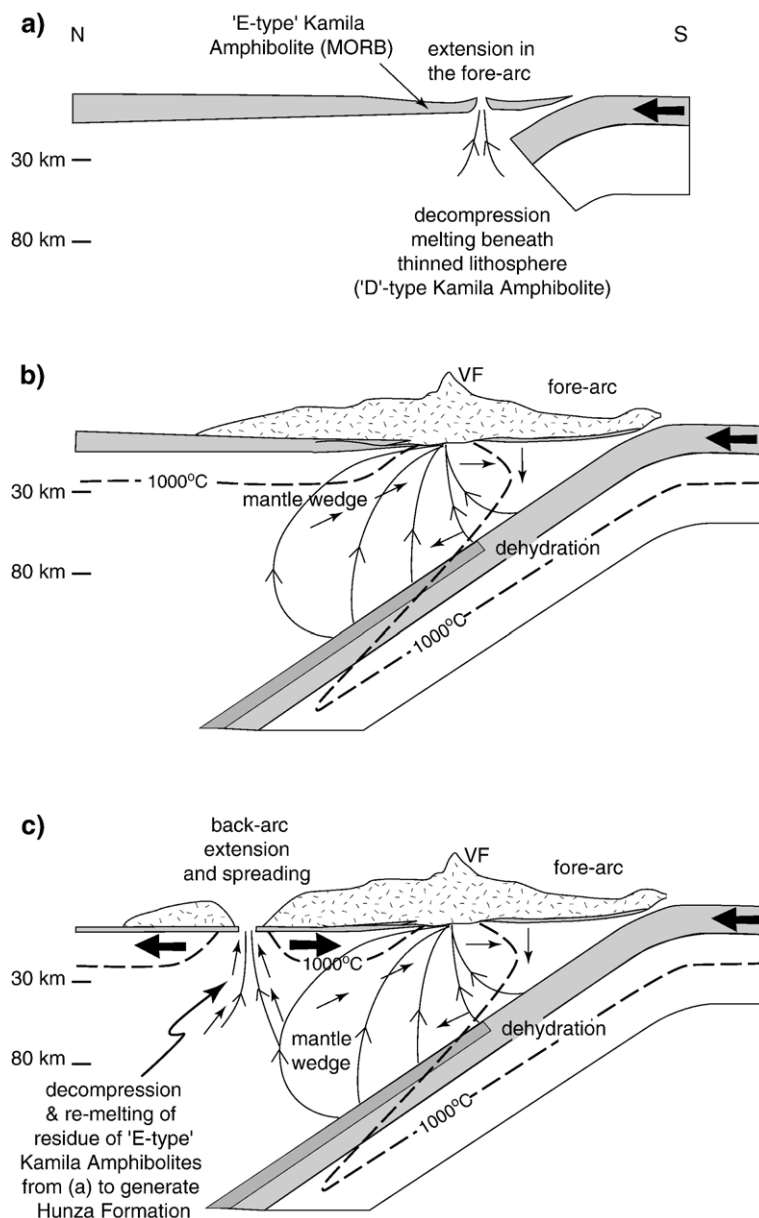


Fig. 13. Schematic diagram showing: (a) emplacement of 'D-type' Kamila Amphibolite onto 'E-type' Kamila Amphibolite (MORB) basement following decompression melting at the initiation of subduction; (b) eruption of Jaglot Group and Chalt Volcanic Group, Ghizar Formation, induced by dehydration fluids from the subducting sediments during steady-state subduction; and (c) eruption of the Chalt Volcanic Group, Hunza Formation in the back-arc through decompression and remelting of the residue from the generation of the 'E-type' Kamila Amphibolites following intra-arc rifting and extension (adapted from McCulloch and Gamble, 1991). Convection lines show possible paths of hydrous fluids and melts in the mantle wedge. VF= volcanic front. Not to scale.

(Fig. 10a). The remaining residue of this primitive mantle source has REE concentrations similar to LREE-depleted spinel lherzolite xenoliths found in the European Alps (Loubet et al., 1975). It is possible, if unlikely, that MORB could be generated from an LREE-depleted lherzolite mantle source. REE modelling of such a source shows that rocks with REE compositions

similar to N-MORB can be produced with only 2% batch partial melting (Fig. 14a). However, melting of this source could not have generated the 'E-type' Kamila Amphibolites (Fig. 14b).

The data presented here are consistent with the hypothesis that the main arc volcanic rocks of the Kohistan arc were erupted above a north-dipping

subduction zone. On the assumption that spinel lherzolite was present in the mantle wedge between about 30 and 80 km depth (10–25 kbar), with garnet lherzolite mantle present at depths >80 km (>25 kbar), the implication is that the main arc volcanic rocks of Kohistan were generated by partial melting of a fertile mantle source (Fig. 13b). The ‘D-type’ mafic rocks of the Kamila Amphibolites, the earliest arc volcanic rocks, were produced at relatively shallow depths, and the mafic rocks of the Jaglot Group and the Ghizar Formation of the Chalt Volcanic Group were generated at depths greater than 80 km as a north-dipping subducting slab penetrated further into the mantle (Fig. 13b).

Petterson and Treloar (2004) argued, on stratigraphic criteria, that the Ghizar and Hunza Formations are coeval units and that it is likely that they were erupted contemporaneously. However, their chemistries are significantly different, and REE modelling indicates very different source materials for them. The basalts and andesites of the Hunza Formation do not fit on the trend displayed by the basaltic rocks of the evolving juvenile arc, including the Ghizar Formation (Fig. 12). If this is so, the Chalt Volcanic Group was formed by two different, adjacent, mantle source regions which must have been active at the same time.

The Hunza Formation of the Chalt Volcanic Group has a MORB-type composition, but also carries a weak arc signature. Models of mantle melting (Fig. 11a, b, c) show that the mafic rocks of the Hunza Formation must have been produced through melting of an LREE-

depleted spinel lherzolite. A possible source would be an Alpine-type LREE-depleted lherzolite (Loubet et al., 1975) which has undergone a previous melting event. In the specific setting of the Kohistan arc rocks, the source could more likely be the residue that remained of the primitive mantle-type source from which the ‘E-type’ Kamila Amphibolites were generated through 6% partial melting (Fig. 11d, e, f).

A two-stage model is indicated. The ‘E-type’ Kamila Amphibolites were generated through partial melting of a primitive mantle source (Fig. 10a) in an intraoceanic setting (Fig. 14a) and form the basement to the whole arc. We suggest that the residue which, after melting, would have REE concentrations similar to those of Alpine peridotites (Loubet et al., 1975) was subsequently underplated beneath the arc and was later remelted as the source for the basalts of the Hunza Formation. This is consistent with field data which suggest that the Kamila Amphibolites form the basement to the arc and that the Hunza Formation with its MORB-like chemistry and weak arc signature is the youngest sequence in the Kohistan arc (Petterson and Treloar, 2004).

Because high-Mg andesites and boninites are most commonly recognised as occurring in the fore-arc, the presence of primitive, high-Mg rocks in the Hunza Formation led Khan et al. (1997) to propose, while not taking account of the high stratigraphic position of these rocks, that they represent the fore-arc, and that they were emplaced above a south-dipping subduction zone. While boninites and high-Mg volcanic rocks are

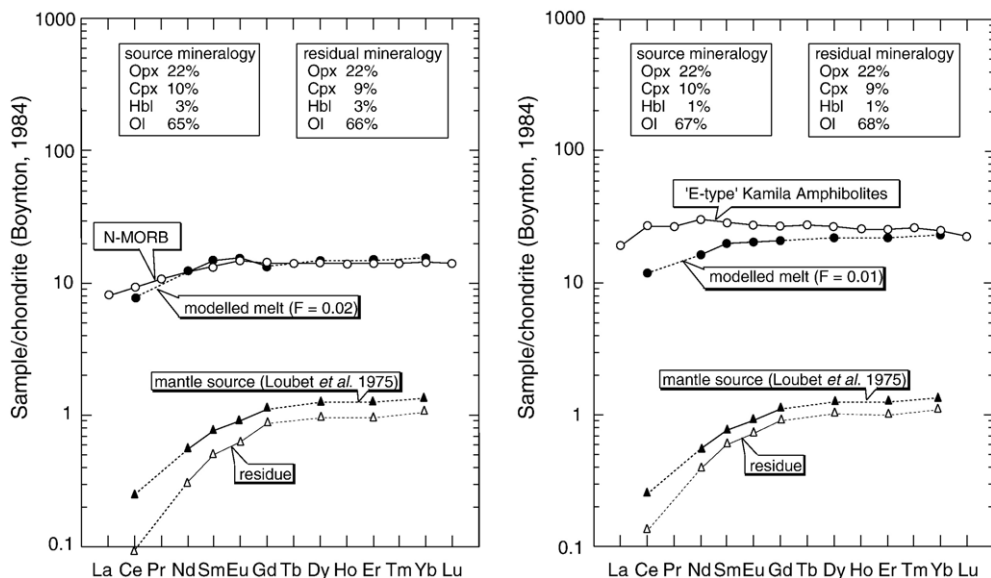


Fig. 14. Mantle melting models for (a) N-MORB and (b) ‘E-type’ Kamila Amphibolites generated from batch partial melting of a mantle source with similar REE concentrations to depleted lherzolite xenoliths from the European Alps (Loubet et al., 1975).

known to be erupted in fore-arc settings (e.g., Crawford et al., 1989; Bloomer et al., 1995), there is a growing body of evidence that shows that they can also be erupted in back-arc settings (e.g., Falloon et al., 1992; Meffre et al., 1996). The high stratigraphic position of the boninites of the Hunza Formation, and their restricted spatial range in the north of the Kohistan arc, is consistent with them being erupted into an intra- or back-arc basin (Clift, 1995; Bédard et al., 1998), and with the arc being erected above a north-dipping subduction zone.

Here, we argue that the rocks of the Hunza Formation were erupted into a back-arc basin. Rifting and opening of the back-arc basin occurred shortly before the arc sutured to Asia. Initial rifting probably occurred behind the volcanic front as a consequence of extension. The first magmas to be erupted were low-Si, low-Mg, magmas with weak arc signatures. These magmas were derived from melting the residue of the primitive mantle source from which the 'E-type' Kamila Amphibolites had been extracted. As rifting progressed, further magmatism occurred. These magmas were the high-Mg basalts, high-Mg andesites and boninites of the Hunza Formation sequence, which also carry only weak arc signatures. We note that boninites constitute only a minor part of this compositionally variable suite of basalts and andesites. The presence of high-Mg basalts and andesites and boninitic units in this region indicates that there was a localised high mantle heat flow. The source of this enhanced heat flow could have been the northward subduction of an active spreading centre (Bignold and Treloar, 2003). However, it is more likely to have been the result of upwelling, hot residual mantle as a result of lithospheric extension associated with rifting and opening of the back-arc basin. Generation of the high-Mg volcanic rocks would thus have been a result of decompression melting of this upwelling mantle material. Following the, probably, short-lived volcanic activity, an active spreading centre began to develop within the rifted basin and normal MORB-type volcanism commenced (Fig. 13c), the arc signature diminishing with time and distance from the trench. That the Hunza Formation carries a weak arc signature indicates connection with, but distance from, the subduction zone.

On the basis of preliminary geochemical analyses Rolland et al. (2002) suggested that basalts from the northern margin of the Ladakh arc, to the immediate east of the Nanga Parbat syntaxis, have a back-arc signature. These basalts are the lateral equivalents of the Hunza Formation, and it is thus likely that they help define a remnant back-arc basin that extends from Ladakh in the east to the present-day Naltar Valley in the west (Figs. 1,

4). This basin was probably restricted along strike length and was short-lived, as its evolution was terminated by closure of the basin during suturing of the Kohistan arc to Asia. The geochemical data presented both here and by Rolland et al. (2002) are consistent with evidence, from the sedimentary record, for extension and rifting that shortly predated collision of Kohistan with Asia (Robertson and Collins, 2002).

6. Conclusions

The Kohistan arc offers almost unique access to a complete stratigraphic succession of an intraoceanic island arc. Geochemistry, isotopic data and REE modelling in this study, despite the fact that the rocks have been metamorphosed, offer the opportunity to identify sources of magma generation beneath the arc which may be used as a model for other intraoceanic island arc volcanoes. Despite the assumptions that had to be made, the results are consistent with models of oceanic island arc formation where magma is drawn initially from spinel-bearing mantle and, that as an arc matures and the subducting slab penetrates deeper into the mantle, magma is generated from a garnet-bearing source. A two-stage model is also proposed, where a mantle source, depleted from a previous melting event, may be underplated and later remelted as a consequence of arc rifting, and erupted as back-arc magma.

Acknowledgements

SMB wishes to thank Professor Brian Windley at the University of Leicester for the loan of rock samples and Professor M. Asif Khan at the National Centre of Excellence, Peshawar University, Pakistan, for providing assistance in the field and for supplying powders for geochemical analysis. Staff at the NERC ICP-MS Facility are thanked for their assistance, with the geochemical analyses under grant No. ICP/89/1295, as are staff at NIGL, Keyworth, UK, for the use of their facilities for isotope analysis under grant No. IP/596/0499. This manuscript has been improved by helpful comments from Roberta Rudnick, Yann Rolland and an anonymous reviewer. [RR]

References

- Ahmed, Z., Chaudhry, M.N., 1976. Petrology of the Babusar area, Diamir district, Gilgit, Pakistan. *Geol. Bull. Punjab Univ.* 12, 67–78.
- Ahmed, Z., Hussain, S., Awan, A., 1977. Petrology of the Thelichi area, Gilgit Agency. *Geol. Bull. Punjab Univ.* 14, 27–38.
- Anczkiewicz, R., Vance, D., 2000. Isotopic constraints on the evolution of metamorphic conditions in the Jijal–Patan complex

- and the Kamila Belt of the Kohistan arc, Pakistan Himalaya. In: Khan, M.A., Treloar, P.J., Searle, M.P., Jan, M.Q. (Eds.), *Tectonics of the Nanga Parbat Syntaxis and the Western Himalaya*. Geol. Soc. London Spec. Publ., vol. 170, pp. 321–331.
- Bédard, J.H., Lauzière, K., Tremblay, A., Sangster, A., 1998. Evidence for forearc seafloor-spreading from the Betts Cove ophiolite, Newfoundland: oceanic crust of boninitic affinity. *Tectonophysics* 284, 23–245.
- Bignold, S.M., Treloar, P.J., 2003. Northward subduction of the Indian Plate beneath the Kohistan island arc, Pakistan Himalaya: new evidence from isotopic data. *J. Geol. Soc. (Lond.)* 160, 377–384.
- Bloomer, S.H., Taylor, B., MacLeod, C.J., Stern, R.J., Fryer, P., Hawkins, J.W., Johnson, L., 1995. Early arc volcanism and the ophiolite problem: a perspective from drilling in the western Pacific. In: Taylor, B., Natland, J. (Eds.), *Active Margins and Marginal Basins of the Western Pacific*. Am. Geophys. Union, Geophys. Monogr., vol. 88, pp. 1–30.
- Boynton, W.V., 1984. Geochemistry of the rare earth elements: meteorite studies. In: Henderson, P. (Ed.), *Rare Earth Element Chemistry*. Elsevier, Amsterdam, pp. 63–114.
- Burg, J.P., Bodinier, J.L., Chaudhry, S., Hussain, S., Dawood, H., 1998. Infra-arc mantle-crust transition and intra-arc mantle diapirs in the Kohistan Complex (Pakistani Himalaya): petrostructural evidence. *Terra Nova* 10, 74–80.
- Cameron, W.E., Nisbet, E.G., Dietrich, V.J., 1979. Boninites, komatiites and ophiolitic basalts. *Nature* 280, 550–553.
- Clift, P.D., 1995. Volcaniclastic sedimentation and volcanism during the rifting of western Pacific backarc basins. In: Taylor, B., Natland, J. (Eds.), *Active Margins and Marginal Basins of the Western Pacific*. AGU, Geophys. Monogr., vol. 88, pp. 67–96.
- Corfield, R.I., Searle, M.P., Pedersen, R.B., 2001. Tectonic setting, origin, and subduction history of the Spontang ophiolite, Ladakh Himalaya, NW India. *J. Geol.* 109, 715–736.
- Coward, M.P., Jan, M.Q., Rex, D., Tarney, J., Thirlwall, M., Windley, B.F., 1982. Geo-tectonic framework of the Himalaya of N. Pakistan. *J. Geol. Soc. (Lond.)* 139, 299–308.
- Coward, M.P., Windley, B.F., Broughton, R.D., Luff, I.W., Petterson, M.G., Pudsey, C.J., Rex, D.C., Khan, M.A., 1986. Collision tectonics in the NW Himalayas. In: Coward, M.P., Ries, A.C. (Eds.), *Collision Tectonics*. Geol. Soc. London Spec. Publ., vol. 19, pp. 203–219.
- Coward, M.P., Butler, R.W.H., Khan, M.A., Knipe, R.J., 1987. The tectonic history of Kohistan and its implications for Himalayan structure. *J. Geol. Soc. (Lond.)* 144, 377–391.
- Crawford, A.J., Falloon, T.J., Green, D.H., 1989. Classification, petrogenesis and tectonic setting of boninites. In: Crawford, A.J. (Ed.), *Boninites and Related Rocks*. Unwin Hyman, pp. 1–49.
- Falloon, T.J., Malahoff, A., Zonenshain, L.P., Bogdanov, Y., 1992. Petrology and geochemistry of back-arc basin basalts from Lau Basin spreading ridges at 15°, 18° and 19°S. *Min. Pet.* 47, 1–35.
- Frey, F.A., Suen, J.C., Stockman, H.W., 1985. The Ronda high temperature peridotite: geochemistry and petrogenesis. *Geochim. Cosmochim. Acta* 49, 2469–2491.
- George, M.T., Harris, N.B.W., Butler, R.W.H., 1993. The tectonic implications of contrasting granite-magmatism between the Kohistan island arc and the Nanga Parbat–Haramosh Massif, Pakistan Himalaya. In: Treloar, P.J., Searle, M.P. (Eds.), *Himalayan Tectonics*. Geol. Soc. London Spec. Publ., vol. 74, pp. 173–191.
- Gill, J.B., 1981. *Orogenic Andesites and Plate Tectonics*. Springer-Verlag, Berlin.
- Hanson, G.N., 1980. Rare earth elements in petrogenetic studies of igneous systems. *Annu. Rev. Earth Planet. Sci.* 8, 371–406.
- Hickey, R.L., Frey, F.A., 1982. Geochemical characteristics of boninite series volcanics: implications for their source. *Geochim. Cosmochim. Acta* 46, 2099–2115.
- Jan, M.Q., 1970. Petrography of the upper part of Kohistan and southwestern Gilgit agency along the Indus and Kandia rivers. *Geol. Bull. Univ. Peshawar* 5, 27–48.
- Jan, M.Q., 1979. Petrography of pyroxene granulites from northern Swat and Kohistan. *Geol. Bull. Univ. Peshawar* 11, 65–87.
- Jan, M.Q., 1988. Geochemistry of amphibolites from the southern part of the Kohistan arc, N. Pakistan. *Min. Mag.* 52, 147–159.
- Jan, M.Q., Howie, R.A., 1981. The mineralogy and geochemistry of the metamorphosed basic and ultrabasic rocks of the Jijal complex, Kohistan, NW Pakistan. *J. Petrol.* 22, 85–126.
- Jan, M.Q., Mian, I., 1971. Preliminary geology and Petrography of Swat Kohistan. *Geol. Bull. Univ. Peshawar* 6, 1–32.
- Jan, M.Q., Tahirkheli, A.Z., 1990. The Tora Tigga Complex, southern Dir, NW Pakistan: an example of mafic–ultramafic rocks in the bottom of an island arc. *Geol. Bull. Univ. Peshawar* 23, 231–251.
- Jan, M.Q., Windley, B.F., 1990. Chromian spinel-silicate chemistry in ultramafic rocks of the Jijal complex, northwest Pakistan. *J. Petrol.* 31, 667–715.
- Jan, M.Q., Banaras, M., Ghani, A., Asif, M., 1983. The Tora Tigga ultramafic complex, southern Dir district. *Geol. Bull. Univ. Peshawar* 16, 11–29.
- Jan, M.Q., Khan, M.A., Windley, B.F., 1992. Exsolution in Al-Cr-Fe₃₊-rich spinel from the Chilas mafic–ultramafic complex, Pakistan. *Am. Min.* 77, 1074–1079.
- Jan, M.Q., Khan, M.A., Qazi, M.S., 1993. The Sapat mafic–ultramafic complex, Kohistan arc, North Pakistan. In: Treloar, P.J., Searle, M.P. (Eds.), *Himalayan Tectonics*. Geol. Soc. London Spec. Publ., vol. 74, pp. 113–121.
- Kelemen, P.B., Hanghøj, K., Greene, A.R., 2003. One view of the geochemistry of subduction-related magmatic arcs, with an emphasis on primitive andesite and lower crust. In: Rudnick, R.L. (Ed.), *Treatise on Geochemistry*, vol. 3, pp. 593–659.
- Kempton, P.D., 1995. Common Pb chemical procedures for silicate rocks and minerals, methods of data correction and an assessment of data quality at the NERC Isotope Geosciences Laboratory. NERC Isotope Geosciences Laboratory Report Series, vol. 78.
- Kempton, P.D., Downes, H., Sharkov, E.V., Vetrin, V.R., Ionov, D.A., Carswell, D.A., Beard, A., 1995. Petrology and geochemistry of xenoliths from the Baltic Shield: evidence for partial melting and metasomatism in the lower crust beneath an Archean Terrane. *Lithos* 36, 157–184.
- Khalil, M.A., Afridi, A.G.K., 1979. The geology and petrography of Doshi–Diwanger area, Ushu Gol Valley, Swat Kohistan. *Geol. Bull. Univ. Peshawar* 11, 99–111.
- Khan, M.A., Jan, M.Q., Windley, B.F., Tarney, J., Thirlwall, M.F., 1989. The Chilas mafic–ultramafic igneous complex; the root of the Kohistan island arc in the Himalaya of Northern Pakistan. In: Malinconico, L.L., Lillie, J. (Eds.), *Tectonics of the Western Himalayas*. Geol. Soc. Am. Spec. Paper, vol. 232, pp. 75–94.
- Khan, M.A., Jan, Q.M., Weaver, B.L., 1993. Evolution of the lower arc crust in Kohistan, N. Pakistan: temporal arc magmatism through early, mature and intra-arc rift stages. In: Treloar, P.J., Searle, M.P. (Eds.), *Himalayan Tectonics*. Geol. Soc. London Spec. Publ., vol. 74, pp. 123–128.

- Khan, T., Khan, M.A., Jan, M.Q., 1994. Geology of a part of the Kohistan terrane between Gilgit and Chilas, northern areas, Pakistan. *Geol. Bull. Univ. Peshawar* 27, 99–112.
- Khan, T., Khan, M.A., Jan, M.Q., Naseem, M., 1996. Back-arc basin assemblages in Kohistan, Northern Pakistan. *Geodin. Acta (Paris)* 9, 30–40.
- Khan, M.A., Stern, R.J., Gribble, R.F., Windley, B.F., 1997. Geochemical and isotopic constraints on subduction polarity, magma sources and palaeogeography of the Kohistan intra-oceanic arc, Northern Pakistan Himalaya. *J. Geol. Soc. (Lond.)* 154, 935–946.
- Khan, M.A., Treloar, P.J., Khan, M.A., Khan, T., Qazi, M.S., Jan, M.Q., 1998. Geology of the Chalt–Babusar transect, Kohistan terrane, N. Pakistan: implications for the constitution and thickening of island arc crust. *J. Asian Earth Sci.* 16, 253–268.
- Loubet, M., Shimizu, N., Allègre, C.J., 1975. Rare earth elements in Alpine peridotites. *Contrib. Mineral. Petrol.* 53, 1–12.
- Mahoney, J.J., Frei, R., Tejada, M.L.G., Mo, X.X., Leat, P.T., Nägler, T.F., 1998. Tracing the Indian Ocean mantle domain through time: isotopic results from Old West Indian, East Tethyan, and South Pacific seafloor. *J. Petrol.* 39, 1285–1306.
- McCulloch, M.T., Gamble, J.A., 1991. Geochemical and geodynamical constraints on subduction zone magmatism. *Earth Planet. Sci. Lett.* 102, 358–374.
- McDonough, W.F., Sun, S.-S., 1995. The composition of the Earth. *Chem. Geol.* 120, 223–253.
- McDonough, W.F., Sun, S.-S., Ringwood, A.E., Jagoutz, E., Hofmann, A.W., 1992. Potassium, rubidium, and cesium in the Earth and Moon and the evolution of the mantle of the Earth. *Geochim. Cosmochim. Acta* 56, 1001–1012.
- Meffre, S., Aitchison, J.C., Crawford, A.J., 1996. Geochemical evolution and tectonic significance of boninites and tholeiites from the Koh ophiolite, New Caledonia. *Tectonics* 15, 67–83.
- Michel, M., Robin, C., Samaniego, P., Hall, M.L., Cotton, J., Mothes, P., Arnaud, N., 1999. Sangay volcano, Ecuador: structural development, present activity and petrology. *J. Volcanol. Geotherm. Res.* 90, 49–79.
- Miller, D.J., Loucks, R.R., Ashraf, M., 1991. Platinum-group element mineralisation in the Jijal layered ultramafic–mafic complex, Pakistan Himalayas. *Econ. Geol.* 86, 1093–1102.
- Miyashiro, A., 1974. Volcanic rock series in island arc series and active continental margins. *Am. J. Sci.* 274, 321–355.
- Pearce, J.A., 1983. Role of the sub-continental lithosphere in magma genesis at active continental margins. In: Hawkesworth, C.J., Norry, M.J. (Eds.), *Continental Basalts and Mantle Xenoliths*. Shiva, Nantwich, pp. 230–249.
- Petterson, M.G., Treloar, P.J., 2004. Volcanostratigraphy of arc volcanic sequences in the Kohistan arc, North Pakistan: volcanism within island arc, back-arc basin, and intra-continental tectonic settings. *J. Volcanol. Geotherm. Res.* 130, 147–178.
- Petterson, M.G., Windley, B.F., 1985. Rb–Sr dating of the Kohistan arc batholith in the trans-Himalaya of North Pakistan, and tectonic implications. *Earth Planet. Sci. Lett.* 74, 45–57.
- Petterson, M.G., Windley, B.F., 1991. Changing source regions of magmas and crustal growth in the trans-Himalayas: evidence from the Chalt volcanics and Kohistan Batholith, Kohistan, Northern Pakistan. *Earth Planet. Sci. Lett.* 102, 326–341.
- Petterson, M.G., Windley, B.F., 1992. Field relations, geochemistry and petrogenesis of the Cretaceous basaltic Jutal dykes, Kohistan, Northern Pakistan. *J. Geol. Soc. (Lond.)* 149, 107–114.
- Petterson, M.G., Windley, B.F., Luff, I.W., 1990. The Chalt volcanics, Kohistan, N Pakistan: High-Mg tholeiitic and low-Mg calc-alkaline volcanism in a Cretaceous island arc. In: Sharma, K.K. (Ed.), *Phys. Chem. Earth* 17, no. II, *Geology and Geodynamic Evolution of the Himalayan Collision Zone*, Part 1, 19–30.
- Petterson, M.G., Crawford, M.B., Windley, B.F., 1993. Petrogenetic implications of neodymium isotope data from the Kohistan Batholith, North Pakistan. *J. Geol. Soc. (Lond.)* 150, 125–129.
- Riley, T.R., Leat, P.T., Pankhurst, R.J., Harris, C., 2001. Origins of large volume rhyolitic volcanism in the Antarctic Peninsula and Patagonia by crustal melting. *J. Petrol.* 42, 1043–1065.
- Robertson, A.H.F., Collins, A.S., 2002. Shyok Suture Zone, N Pakistan: late Mesozoic–Tertiary evolution of a critical suture separating the oceanic Ladakh Arc from the Asian continental margin. *J. Asian Earth Sci.* 20, 309–351.
- Rolland, Y., Pecher, A., Picard, C., 2000. Middle Cretaceous back-arc formation and arc evolution along the Asian margin: the Shyok Suture Zone in northern Ladakh (NW Himalaya). *Tectonophysics* 325, 145–173.
- Rolland, Y., Picard, C., Pecher, A., Lapierre, H., Bosdch, D., Keller, F., 2002. The Cretaceous Ladakh arc of NW Himalaya: slab melting and melt-mantle interaction during fast northward drift of Indian Plate. *Chem. Geol.* 182, 139–178.
- Royse, K.R., Kempton, P.D., Darbyshire, D.P.F., 1998. Procedure for the analysis for rubidium–strontium and samarium–neodymium isotopes at the NERC Isotope Geosciences Laboratory. NERC Isotope Geosciences Laboratory Report Series, vol. 121.
- Sullivan, M.A., 1992. The geology of the roof zone of the Kohistan Batholith, Northwestern Pakistan. Unpublished PhD thesis, University of Leicester.
- Sullivan, M.A., Windley, B.F., Saunders, A.D., Haynes, J.R., Rex, D. C., 1993. A palaeogeographic reconstruction of the Dir Group: evidence for magmatic arc migration within Kohistan, N. Pakistan. In: Treloar, P.J., Searle, M.P. (Eds.), *Himalayan Tectonics*. *Geol. Soc. London Spec. Publ.*, vol. 74, pp. 139–160.
- Sun, S.-S., McDonough, W.F., 1989. Chemical and isotopic systematics of oceanic basalts: implications for mantle composition and processes. In: Saunders, A.D., Norry, M.J. (Eds.), *Magmatism in the Ocean Basins*. *Geol. Soc. London Spec. Publ.*, vol. 42, pp. 313–345.
- Tahirkheli, R.A.K., Mattauer, M., Proust, F., Taponnier, P., 1979. The India–Eurasia suture zone in northern Pakistan: synthesis and interpretation of recent data at plate scale. In: Farah, A., Dejong, K. A. (Eds.), *Geodynamics of Pakistan*. *Geol. Surv., Pakistan, Quetta*, pp. 125–130.
- Treloar, P.J., Rex, D.C., Guise, P.G., Coward, M.P., Searle, M.P., Windley, B.F., Petterson, M.G., Jan, M.Q., Luff, I.W., 1989. K–Ar and Ar–Ar geochronology of the Himalayan collision in NW Pakistan: constraints on the timing of suturing, deformation, metamorphism and uplift. *Tectonics* 8, 881–909.
- Treloar, P.J., Brodie, K.H., Coward, M.P., Jan, M.Q., Khan, M. A., Knipe, R.J., Rex, D.C., Williams, M.P., 1990. The evolution of the Kamila shear zone, Kohistan, Pakistan. In: Salisbury, M.H., Fountain, D.M. (Eds.), *Exposed Cross-sections of the Continental Crust*. Kluwer Academic Press, Amsterdam, pp. 175–214.
- Treloar, P.J., Petterson, M.G., Jan, M.Q., Sullivan, M.A., 1996. A re-evaluation of the stratigraphy and evolution of the Kohistan arc sequence, Pakistan Himalaya: implications for magmatic and tectonic arc building processes. *J. Geol. Soc. (Lond.)* 153, 681–693.
- Wood, B.J., Fraser, D.G., 1986. *Elementary Thermodynamics for Geologists*. Oxford University Press.

- Yamamoto, H., Nakamura, E., 1996. Sm–Nd dating of garnet granulites from the Kohistan complex, northern Pakistan. *J. Geol. Soc. (Lond.)* 153, 965–969.
- Yamamoto, H., Nakamura, E., 2000. Timing of magmatic and metamorphic events in the Jijal complex of the Kohistan arc deduced from Sm–Nd dating of mafic granulites. In: Khan, M.A., Treloar, P.J., Searle, M.P., Jan, M.Q. (Eds.), *Tectonics of the Nanga Parbat Syntaxis and the Western Himalaya*. Geol. Soc. London Spec. Publ., vol. 170, pp. 313–319.
- Zeilinger, G., Burg, J.-P., Schaltegger, U., Seward, D., 2001. New U/Pb and fission track ages and their implication for the tectonic history of the lower Kohistan arc complex, northern Pakistan. *J. Asian Earth Sci.* 19, 79–80.
- Zeitler, P.K., Tahirkheli, R.A.K., Naesser, C., Johnson, N., Lyons, J., 1981. Preliminary fission track ages from the Swat valley, northern Pakistan. *Geol. Bull. Univ. Peshawar* 13, 63–65.